2013-12-13

An Experimental Analysis of the Weighted Sum of Spatial Gradients Minimization Quantity in Active Structural Acoustic Control of Vibrating Plates

Daniel R. Hendricks
Brigham Young University - Provo

An Experimental Analysis of the Weighted Sum of Spatial Gradients Minimization Quantity in Active Structural Acoustic Control of Vibrating Plates

Daniel R. Hendricks

A thesis submitted to the faculty of
Brigham Young University
in partial fulfillment of the requirements for the degree of

Master of Science

Jonathan D Blotter, Chair
Scott D. Sommerfeldt
Kent L. Gee

Department of Mechanical Engineering

Brigham Young University

December 2013

ABSTRACT

An Experimental Analysis of the Weighted Sum of Spatial Gradients
Minimization Quantity in Active Structural
Acoustic Control of Vibrating Plates

Daniel R. Hendricks
Department of Mechanical Engineering, BYU
Master of Science

Active Structural Acoustic Control (ASAC) is a subcategory of the more widely known field of Active Noise control (ANC). ASAC is different from traditional ANC methods because it seeks to attenuate noise by altering the noise producing structure instead of altering the acoustic waves traveling through the air. The greatest challenge currently facing ASAC researchers is that a suitable parameter has not yet been discovered which can be easily implemented as the minimization quantity in the control algorithms. Many parameters have been tried but none effectively attenuate the sound radiation in a way that can be easily implemented. A new parameter was recently developed which showed great potential for use as a minimization quantity. This parameter has been termed the "weighted sum of spatial gradients" (WSSG) and was shown by previous researchers to significantly reduce noise emissions from a vibrating simply supported plate in computer simulations. The computer simulations indicate that WSSG-based control provides as good or better control than volume velocity and does so with a single point measurement which is relatively insensitive to placement location. This thesis presents the experimental validation of the WSSG computer simulations. This validation consists of four major components. First, additional research was needed in to extend the use of WSSG from computer simulations to experimental setups. Second, the WSSG-based control method was performed on simply supported plates to validate the computer simulations. Third, the WSSG-based control method on was used on clamped plates to validate the computer simulations, and fourth, the WSSG-based control method was validated on plates with ribs. The important results are discussed and conclusions summarized for each of these sections. Recommendations are made for future work on the WSSG parameter.

Keywords: ASAC, ANC, vibration control, active control of structures, independent radiation modes, experimental WSSG, simply supported plate, clamped plate, ribbed plate, Daniel R. Hendricks.

ACKNOWLEDGEMENTS

First and foremost, I would like to recognize the fact that the research presented in this thesis would not have been possible without help from many people who sacrificed their time and talents to help me along my way. I was blessed to be surrounded by great minds who provided much needed insights and directions as I made my way through this process. My graduate committee chair, Dr. Jonathan Blotter, and committee members, Dr. Scott Sommerfeldt and Dr. Kent Gee were especially helpful and I owe them a great debt of gratitude. The material presented here never would have happened if not for their guidance and continued patience with me.

I would also like to thank several fellow researchers who worked with me and provided a valuable resource to bounce ideas off and collaborate with on difficult subjects. These include Pegah Aslani, Yin Cao, and William Johnson. Much of my thesis work would not have been possible without help from William and the work which he performed in order to advance our theoretical knowledge of the WSSG parameter.

Although these men and women provided valuable help with my research, the person for whom I am most grateful in my life is my wonderful wife, Sharlee. I would like to thank her for letting me spend many long nights at work completing this thesis and for putting up with the uncertainties that came with it.

I would lastly look heavenward and recognize many instances when unbidden inspiration came to help me through this work.

This work was supported by a grant from the National Science Foundation, NSF CMMI-1130482.

TABLE OF CONTENTS

LIST OF TABLES

LIST OF FIGURES

1 INTRODUCTION

This chapter presents an introduction to active structural acoustic control (ASAC) and highlights some of the important contributions from other researchers. The "weighted sum of spatial gradients" (WSSG) quantity is defined and simulations are presented that demonstrate how WSSG is used in ASAC situations. This is done to provide context for the remainder of the thesis. The problem statement is then given and the remainder of the thesis outlined.

1.1 Active Noise Control and Active Structural Acoustic Control

ASAC is an important subcategory of the larger field of active noise control (ANC). ANC is a process by which a sensor is used to measure a certain aspect of an acoustic field and then a secondary sound source is used to minimize that aspect. This minimization is often achieved by the superposition of waves, modal control or modal rearrangement, and is done with the hopes of attenuating the noise levels in the air. Local and/or global attenuation is possible depending on which quantity is being controlled. These methods are generally used in situations when passive noise control methods are either ineffective or unusable.

To implement ANC three major components are needed: a sensor(s), a control algorithm, and a second sound source (actuator). The sensor(s) measures the desired parameter and passes the information to the control algorithm. The control algorithm uses the information to calculate the proper signal for the actuator. The actuator then emits a new signal which drives the measurement at the sensor(s) to a minimum. This process is then repeated continuously.

ASAC uses the same process as ANC, but with one key difference; ANC attempts to minimize noise through interactions of the sound waves in the air, while ASAC attempts to minimize radiated sound power by exerting control on the noise producing structure. This gives ASAC a significant advantage over ANC because ASAC is able to target the sound right at its point of generation rather than after it has propagated in all directions. Global control is thus obtained in many ASAC situations. Additionally, in ASAC systems, the actuators are applied directly to the noise radiating structure. This is another key benefit which it has over ANC, which relies on control actuators located out in the acoustic field. This can be cumbersome and intrusive. ASAC avoids this by placing the actuators directly on the structure, thus saving space and minimizing the intrusions into the acoustic field. A schematic of a typical ASAC system is shown in Figure 1-1.

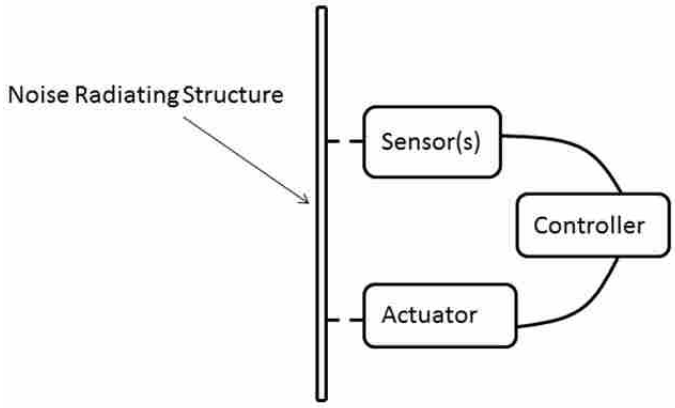

Figure 1-1: Schematic of an ASAC System

1.2 Literature Review

One of the main limitations currently facing ASAC researchers is that an ideal parameter has not yet been discovered which can be easily implemented as the minimization quantity. This parameter must be measureable directly on the vibrating structure and be correlated to the sound

radiation from the vibrating structure in such a way that minimizing the quantity would also minimize the radiated sound. Several parameters have been attempted but most have been shown to be ineffective or cumbersome to use. The rest of this section will briefly review some of these other parameters and relevant research conducted by other ASAC researchers.

Snyder and Hansen[1] demonstrated that there are two main methods used to control noise from a radiating finite structure: modal control and modal rearrangement. Modal control is achieved by minimizing the amplitudes of the structural modes. Doing so will decrease the total volume velocity of the plate and thus attenuate sound radiation. Modal rearrangement is done by altering the number, phase, and amplitudes of the structural modes in such a way that the plate is no longer an efficient radiator. An example of this could be changing an efficiently radiating 1-3 structural mode to a less efficient 1-2 or a 1-4 mode (Fahy[2] shows that even structural modes radiate less efficiently than odd structural modes when ka (acoustic wave number times plate width) is small due to intercell cancellation). An effective ASAC situation could utilize either or both of these methods to create attenuation.

Early efforts on ASAC looked at placing the minimization sensor in the acoustic field and placing the actuators directly on the structure. Pan, Snyder and Hansen[3] looked at minimizing the far field sound pressure, sound pressure at a single point, and total radiated sound power by applying a vibration source on the plate. It was demonstrated experimentally that controlling sound pressure at a single point with a vibration source on the plate does attenuate noise in many instances. Similar results were seen in other papers by Fuller *et al.*[4, 5]. While these results showed that it was possible to attenuate noise coming from a structure with vibration sources, they were accomplished using acoustic minimization parameters located out in the acoustic field. This is

often not ideal for practical situations and recent research has been focused on finding a parameter which can be measured directly on the surface of the structure.

Snyder and Tanaka[6] show that "minimizing the velocity of structural modes is not… always the best approach to minimizing acoustic radiation from the structure." Minimizing the velocity of the structural modes *can* produce attenuation but requires *a priori* knowledge of the structural mode shapes in order to place vibration sensors directly on the apex of the anti-nodes. Minimizing all the anti-nodes is also difficult to do with a limited number of control actuators because minimizing one anti-node will often cause an amplification of others. It has also been shown that increasing the velocity of the anti-nodes *can* actually produce a reduction in sound radiation if it achieves a modal rearrangement[1, 3], and vice-versa. Thus the use of the structural mode velocities is not an ideal minimization quantity for use in ASAC situations.

Snyder and Tanaka[6] present a method of using shaped piezo-electric polymer film sensors to measure weighted sets of orthogonal modes as the error signal in ASAC situations. This is shown to provide global sound attenuation at low frequencies, but it also requires *a priori* knowledge of the vibrating structure and an optimization of the weights for each structural mode.

Elliot *et al.*[7, 8, 9] have done extensive research on the use of volume velocity as the minimization parameter in ASAC situations. This was done by placing an array of accelerometers on the surface of the plate and estimating the overall volume velocity by summing the accelerometer outputs. Minimizing volume velocity is shown to achieve attenuation in certain instances but several drawbacks exist. The primary drawback relates to the number of sensors required to accurately estimate the overall volume velocity of the vibrating structure. Sors and Elliott[7] show that the number of sensors needed to acquire a good estimate of the volume velocity is given by

$$N = \frac{5}{3\pi} cl \left(\frac{m}{D}\right)^{\frac{1}{2}} \quad (1\text{-}1)$$

where c is the speed of sound, l is the smallest plate dimension, D is the bending stiffness and m is the mass per unit area. This means that for a steel rectangular plate whose smallest dimension is 0.483 meters, the approximate number of sensors should be 62[10]. This is impractical for experimental situations. Minimizing volume velocity is also shown to be ineffective for even numbered structural modes. Even number structural modes have an equal amount of mass moving in the positive direction as the negative direction and so has a net volume velocity of zero. These drawbacks limit the effectiveness of volume velocity as a minimization quantity in ASAC situations.

Several other structural based parameters have been attempted for use in ASAC situations. Structural intensity, or power flow, has been shown to have little effect on acoustic intensity[11] and thus was not suited for ASAC situations. Controlling independent radiation modes has been shown to be effective but requires many sensors and *a priori* knowledge of the important radiation modes of the noise being produced[12, 13, 14]. This is often impractical for many situations where measurements and calculations would need to be made for each new situation.

1.3 **Weighted Sum of Spatial Gradients**

Recently, a new parameter was developed by Fisher *et al.*[15] that showed great potential as a minimization quantity that could attenuate sound levels with relatively easy implementation. This parameter consists of the sum of the squared transverse motion, w, and the squared spatial derivatives, $\frac{\partial w}{\partial x}$, $\frac{\partial w}{\partial y}$ and $\frac{\partial^2 w}{\partial x \partial y}$. Fisher *et al.* initially termed the quantity "V_{Comp}" (for composite velocity) since the preliminary equations were based on the spatial derivatives of the velocity

field. This name has been changed to the weighted sum of spatial gradients (WSSG) to more accurately describe the quantity. A brief overview the WSSG derivation and its use in ASAC are given in the next few sections. A more complete derivation is given in by Fisher *et al*[15] publication.

1.3.1 WSSG Derivation

The idea for WSSG came about when researchers began looking for a structural quantity that is uniform across the entire. A spatially uniform quantity would have a significant advantage over other ASAC parameters such as volume velocity and structural velocities because it would require only a single sensor arbitrarily placed on the plate and no *a priori* knowledge of the structure.

It was noted by Fisher *et al.*[15] that the four quantities w (The transverse motion), and the spatial derivatives $\frac{\partial w}{\partial x}$, $\frac{\partial w}{\partial y}$ and $\frac{\partial^2 w}{\partial x \partial y}$ each target different locations on a vibrating simply supported plate. While w represents the displacement in these terms, it should be noted that for time harmonic excitation sources, velocity or acceleration could equally be used in its place. The only difference between using displacement and using either velocity or acceleration is that velocity and acceleration are scaled by the factors $i\omega$ and $(i\omega)^2$ respectively. Figure 1-2 shows simulations of all four terms (squared) for the first structural mode of a vibrating simply supported plate. The four simulations were each normalized so that the same maximum values exist on all plots.

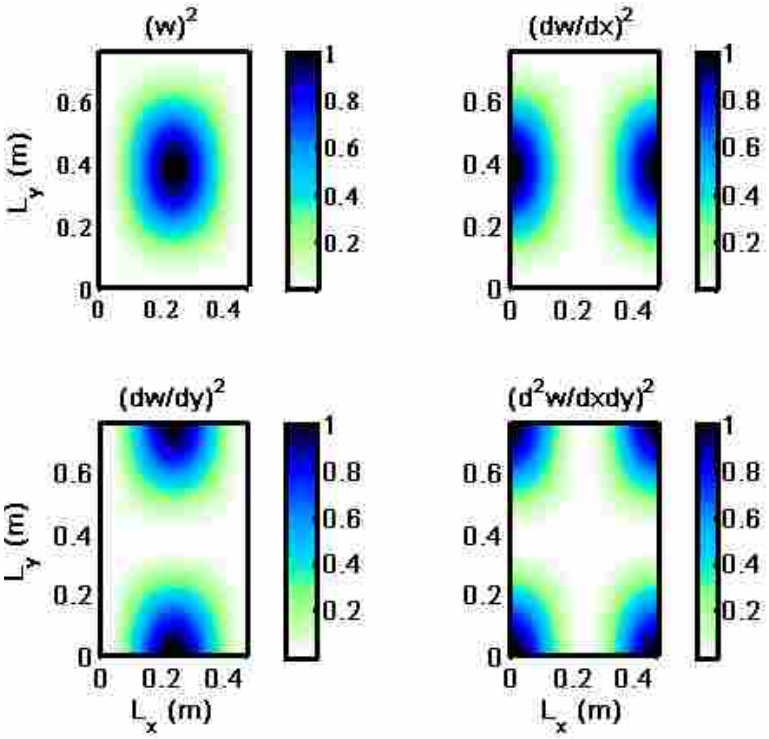

Figure 1-2: Normalized $(w)^2$, $\left(\frac{\partial w}{\partial x}\right)^2$, $\left(\frac{\partial w}{\partial y}\right)^2$ and $\left(\frac{\partial^2 w}{\partial x \partial y}\right)^2$ for the First Structural mode of a Simply Supported Plate

Due to the fact that each of these four terms target different parts of the plate, they can be summed into a single quantity and the result will be a uniform value of "1" across the face of the plate. Figure 1-2 shows these four terms for the first structural mode of a simply supported plate but it was noted that higher modes also exhibit similar results. The individual plots will look different from Fig. 1-2, but the sum of all four normalized terms will still result in a uniform value. WSSG was thus defined as the summation of these four terms, each multiplied by a weighting value as shown in Eq. 1-2.

$$WSSG = \alpha(w)^2 + \beta\left(\frac{\partial w}{\partial x}\right)^2 + \gamma\left(\frac{\partial w}{\partial y}\right)^2 + \delta\left(\frac{\partial^2 w}{\partial x \partial y}\right)^2 \qquad (1\text{-}2)$$

The weighting factors α, β, γ, and δ do not need to normalize the value of WSSG to "1" but they are chosen in such a way that each of the four terms contribute equally to the WSSG quantity.

The factors also include dimensions so that consistent units are maintained between the four terms. It was determined that the weights are dependent upon the structural mode of the plate and new weights should be calculated for each structural mode.

1.3.2 Original WSSG Weighting Factors

The scaling factors (weights) used in WSSG were originally derived using the analytical equations for the displacement of a simply supported plate. The displacement of a simply supported plate can be calculated using Eqs. 1-3 through 1-6,

$$w(x,y) = \sum_{q=1}^{F} \frac{f_q}{\rho_s h} \sum_{m}^{\infty} \sum_{n}^{\infty} \frac{W_{mn}(x,y) W_{mn}(x_q, y_q)[\omega_{mn}^2 - \omega^2 - i\eta\omega_{mn}^2]}{[\omega_{mn}^2 - \omega^2]^2 + \eta^2 \omega_{mn}^4} \tag{1-3}$$

$$W_{mn}(x,y) = \frac{2}{\sqrt{L_x L_y}} sin\left(\frac{m\pi x}{L_x}\right) sin\left(\frac{n\pi y}{L_y}\right) \tag{1-4}$$

$$\omega_{mn} = \sqrt{\frac{D}{\rho_s h}} \left(\frac{m^2\pi^2}{L_x^2} + \frac{n^2\pi^2}{L_y^2}\right) \tag{1-5}$$

$$D = \frac{Eh^3}{12(1-\nu^2)} \tag{1-6}$$

where f_q is the amplitude of the qth driving force located at (x_q, y_q), ρ_s is the density of the plate, E is Youngs modulus, ν is Poisson's ratio, h is the thickness of the plate, and L_x and L_y are the x and y dimensions of the plate respectively.

The weights were calculated by taking the spatial gradients $\frac{\partial w}{\partial x}$, $\frac{\partial w}{\partial y}$ and $\frac{\partial^2 w}{\partial x \partial y}$, and then comparing the results to Eq. 1-3. For example, β was found by examining Eq. 1-7 and noticing that the only difference between its amplitude and the amplitude of Eq. 1-3 was the factor $\left(\frac{m\pi}{L_x}\right)$.

$$\frac{\partial w}{\partial x}(x,y) = \sum_{q=1}^{F} \frac{f_q}{\rho_s h} \sum_{m}^{\infty} \sum_{n}^{\infty} \frac{\frac{2}{\sqrt{L_x L_y}} \cos\left(\frac{m\pi x}{L_x}\right) \sin\left(\frac{n\pi y}{L_y}\right) W_{mn}(x_q, y_q)[\omega_{mn}^2 - \omega^2 - i\eta\omega_{mn}^2]}{[\omega_{mn}^2 - \omega^2]^2 + \eta^2 \omega_{mn}^4} \left(\frac{m\pi}{L_x}\right) \qquad (1\text{-}7)$$

The value of β was thus set to be $\beta = 1/\left(\frac{m\pi}{L_x}\right)^2$, because each of the WSSG terms is squared. A similar process was followed for γ and δ. Table 1-1 gives the values of all four scaling factors.

Table 1-1: Simply Supported Scaling Factors

α	$\beta[m^2]$	$\gamma[m^2]$	$\delta[m^4]$
1	$\left(\frac{L_x}{m\pi}\right)^2$	$\left(\frac{L_y}{n\pi}\right)^2$	$\left(\frac{L_x L_y}{mn\pi^2}\right)^2$

These scaling factors can be used to create a uniform quantity for any single structural mode of a simply supported plate. Later chapters of this thesis will explore these weights further in order to expand their use for multiple frequencies and different boundary conditions.

1.3.3 WSSG as an ASAC Minimization Parameter

Developing WSSG as a uniform quantity was one of the main goals of Fisher *et al.*[15], but in order for WSSG to be useful as a minimization quantity in ASAC situations it must also be correlated to sound radiation from a plate. Minimizing WSSG should minimize the global sound radiation from the plate.

Similarities were noted between the four WSSG terms and the first four independent acoustic radiation modes of the first structural mode of a simply supported plate. Independent acoustic radiation modes are an eigenvalue decomposition of the acoustic field using the method of elementary radiators. Fahy and Gardonio[2] show these acoustic radiation modes are directly related to sound power radiating from a vibrating plate and controlling these modes should result in global attenuation of radiated sound power.

It was theorized that controlling the four WSSG terms would mimic controlling the first four acoustic radiation modes and that doing so would cause an attenuation of radiated sound power. The first four acoustic radiation modes contribute the majority of the radiated sound power at low frequencies, so significant attenuation might be possible to achieve even though only four of these modes are being controlled.

In order to test this hypothesis simulations were created using MATLAB® to investigate the use of WSSG in a control algorithm. A vibrating simply supported plate was modeled using Eqs. 1-3 through 1-6. The properties of the simulated plate are given in Table 1-2 and match the properties of the experimental simply supported plate used in later chapters.

Table 1-2: Properties of the Simply Supported Plate

Property	Value
Length (x direction)(L_x)	0.4731 m
Length (y direction)(L_y)	0.7525 m
Thickness (h)	0.0032 m
Young's modulus (E)	68.9 GPa
Poisson's ratio (ν)	0.334
Density (ρ)	2700 Kg/m^3
Damping ratio (η)	2%

WSSG was calculated at a single point using Eq. 1-2 and a second control force was added to the simulation. The phase and amplitude of this second force was optimized to drive WSSG to a minimum. Sound power was calculated with the controller on and off using the method of elementary radiators[2]. This was repeated for a range of forcing frequencies.

Figure 1-3 shows the results of one of these simulations with the disturbance shaker (F_d), control shaker (F_c) and sensor (S) located at $F_d = (0.397, 0.625)$ m, $F_c = (0.124, 0.467)$ m and $S = (0.146, 0.133)$ m. Fisher *et al.*[15] showed figures similar to Fig. 1-3 in their work but Fig. 1-

3 represents a new simulation created by the author for the purpose of this thesis. This was done so that future experimental work would have a simulation to which comparisons could be made. Figure 1-4 shows the coordinate system used for all plates studied in this thesis.

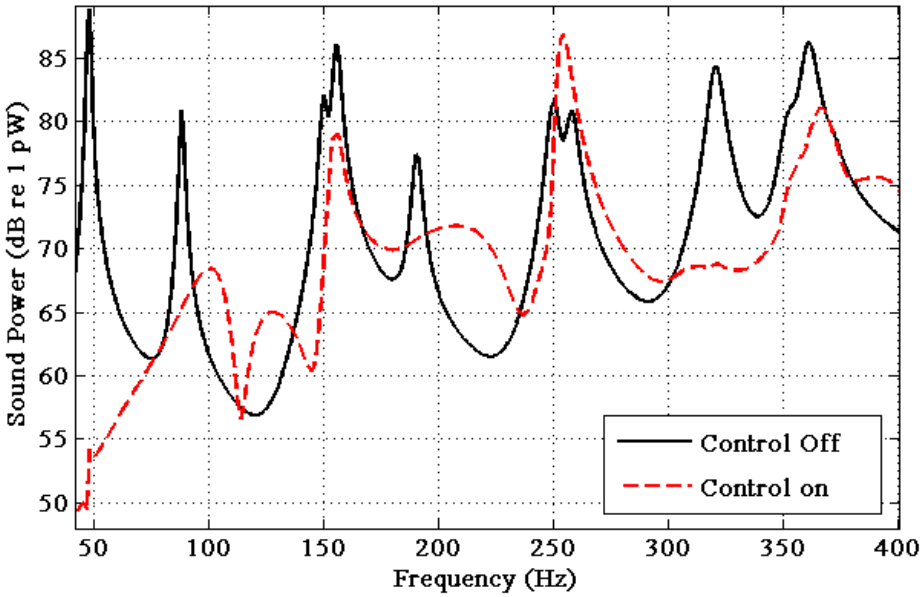

Figure 1-3: Simulated Sound Power Results Using WSSG as a Minimization Parameter

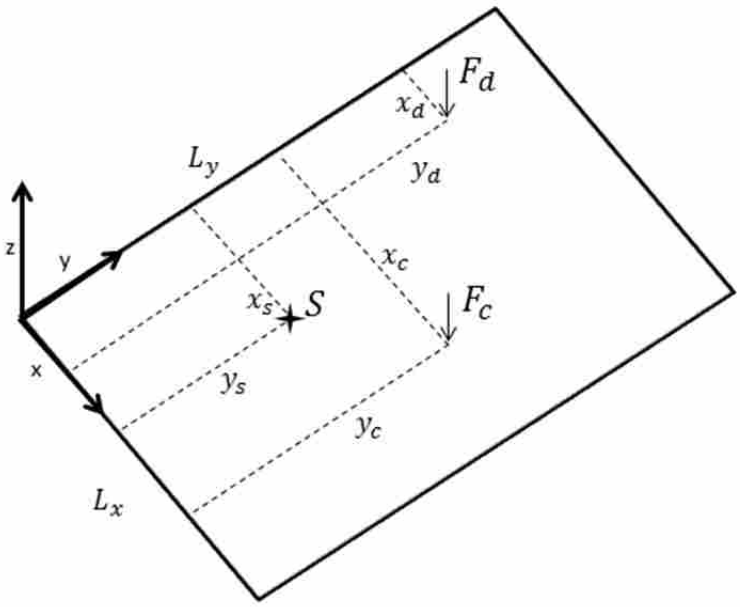

Figure 1-4: Coordinate System for all Plates Studied in this Thesis

On a vibrating plate, the majority of the radiated sound power comes from the resonance frequencies. Resonance causes the amplitudes of the vibrations to increase drastically, generally causing more power to be radiated. Therefore special attention should be placed on the resonance frequencies when attempting to validate the usefulness of WSSG in control situations. Figure 1-3 shows that controlling WSSG attenuates seven of the nine resonance frequencies within this frequency range. There is a slight amplification of radiated power in between most peaks, but these do not contribute to a significant source of overall amplification due to their relatively low levels compared to the peaks. This means that WSSG does a reasonable job of controlling the major sources of noise, but it is not perfect. There are two peaks which are actually amplified, and a few of the peaks are only minimal controlled.

The amplification of radiated power occurs because the control algorithm is not designed to minimize radiated power, but to minimize WSSG. Thus there are a few times when minimizing WSSG at a point actually amplifies the overall radiated power. This means that WSSG may not be a perfect corollary between structural vibrations and radiated sound power. It nonetheless does attenuate many of the resonance peaks and so it may still be useful as a minimization parameter in ASAC situations.

Fisher *et al.*[15] show that results similar to Fig 1-3 are actually comparable to control plots when other ASAC parameters are used as the minimization quantities. The biggest difference between WSSG-based control plots and the other methods is that WSSG-based control is achieved with a single point sensor located on the surface of the plate. Most other ASAC sensors include multiple sensors or sensors located out in the radiated sound field.

1.4 **Thesis Objective**

The work by Fisher *et al.*[15] showed that WSSG had considerable potential for use as the minimization quantity in ASAC situations. However, their work was limited to computer simulations of simply supported flat plates. In order for WSSG to be considered a viable alternative to other common ASAC metrics, it needs to be shown to work in experimental tests and on other types of structures. Thus the problem which this thesis addresses is twofold: first a method needs to be found to measure WSSG in an experimental setup, and second WSSG must then be used in experiments for a variety of structures and boundary conditions.

Figure 1-5 outlines the on-going research on WSSG and highlights the research done for this thesis. The areas in the solid line represent work done by the author and the areas in the dashed lines represent work done jointly with the author and fellow researchers.

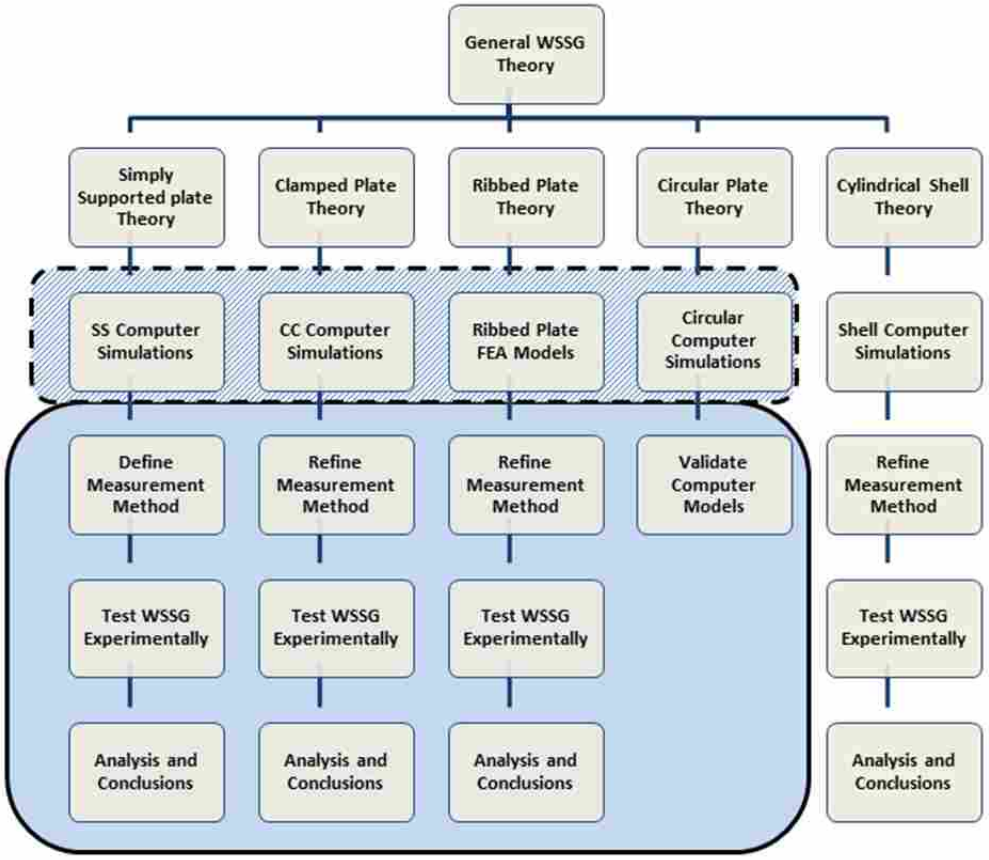

Figure 1-5: Outline of WSSG Research, Highlighting the Author's Contributions

1.5 **Thesis Outline**

The remainder of this thesis presents the research which has been done in order to meet the problem outlined in the section above. Chapter 2 contains additional research which was necessary to complete before experimental work could be done. This includes research on the WSSG theory as well as practical insights on the method selected to measure WSSG. Chapters 3, 4, and 5 present the experimental results for flat simply supported, flat clamped, and ribbed plates respectively. The experimental results are presented, compared to computer simulations, and then discussed. Finally, Chapter 6 gives a summary of the important conclusions and discusses recommendations for future work.

2 ANALYTICAL ANALYSIS OF WSSG AND ADDITIONAL SIMULATIONS

In order to experimentally validate WSSG as a minimization quantity it was first necessary to advance the analytical research which Fisher *et al.*[15] initiated. This additional research is broken into three major sections: a further analysis of the weights, the determination of a method to measure the spatial derivatives, and an analysis of the effects of degenerate modes on WSSG.

2.1 Further Analysis of the Weights.

As noted in Chapter 1, the original weights derived for use in WSSG on simply supported plates are dependent on the structural mode numbers m and n. This means exact weights can be calculated if a plate is vibrating at a single resonant frequency. However, if there are multiple natural frequencies being excited, or if the frequency being excited is not near a natural frequency, then the equations in Table 1-1 have less applicability. Fisher *et al.*[15] recognized this and arbitrarily chose to average the weights over the first 15 modes and use these values in the control algorithm. Using this method they were able to use one set of weights for a range of frequencies and achieve reasonable success in controlling sound radiating from each of the natural frequencies. However, further research was required to determine if this was the best method for calculating weights.

In this work, several new methods for calculating weights were devised and tested using MATLAB® based simulations. It was determined that the two methods which provided the most

overall attenuation were using an average (mean) value calculated over the modes of interest (method "A"), and adapting the weights so that the controller uses the weights of the nearest resonant frequency (method "B"). When the results of these two simulations were plotted together (See Fig. 2-1), it became apparent that there was little difference between the two methods.

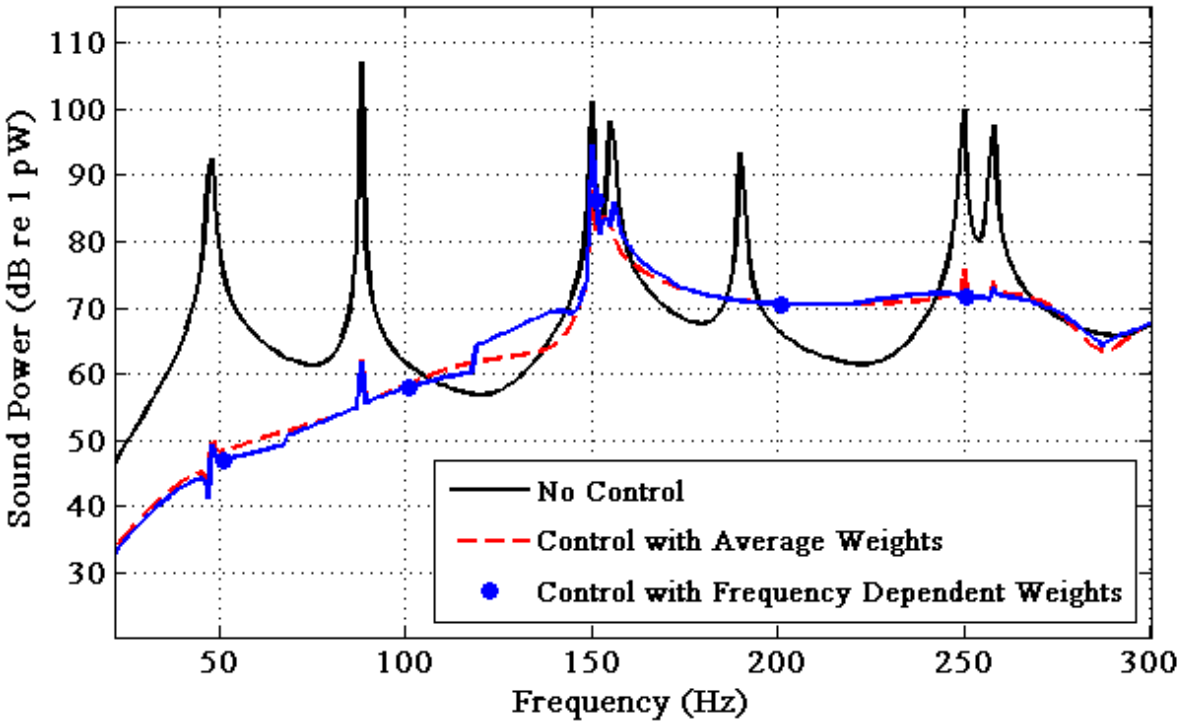

Figure 2-1: Simulated Radiated Power for Two Methods of Calculating WSSG Weights

The simulated results were validated by the author by performing actual experimental tests on a simply supported plate. These tests were performed using the methods described in Chapter 3. The attenuation levels were measured at the resonance frequencies and it was shown that the difference in attenuated sound power levels using method "A" weights and method "B" weights was never more than two tenths of a dB. This implies that the weights used in WSSG are fairly robust and knowing the exact values of the weights out to several significant figures is not

needed. It was determined that getting the correct order of magnitude of the weights is very important but getting the exact value is less so.

This information indicates that small gains could possibly be made using different methods but the gains would be minimal. Therefore, further research on the method of calculating the exact values of the WSSG weights was not pursued. For the remainder of this work an average of the weights over the range of interest will be used in all tests. This means a single value could be calculated for each weight and hard coded into the controller. Using this method, none of the natural frequencies will have a perfectly uniform WSSG field, but they will still be uniform enough to obtain significant sound attenuation.

2.2 **Measuring the Spatial Derivatives**

In order to use WSSG on an experimental plate, a method needed to be devised to measure the four terms used in the summation: w, $\frac{\partial w}{\partial x}$, $\frac{\partial w}{\partial y}$ and $\frac{\partial^2 w}{\partial x \partial y}$. As was noted in Chapter 1, w represents the transverse displacement, but for time harmonic excitation sources the transverse velocity or acceleration could also be used. This thesis focuses on time harmonic excitation sources and so at times velocity or acceleration are used instead of displacement. Many methods, including strain gauges[16], lasers and shaped polyvinylidene fluoride films[17], were explored to measure these derivatives. The best solution based on ease of implementation was determined to be an array of four closely spaced accelerometers. The signals from these accelerometers were combined to form numerical approximations of the derivative terms using the centered difference approximation of the first derivative. A schematic of the accelerometer array is shown in Fig. 2-2, with the corresponding numerical derivatives in Eqs. 2-1 through 2-4.

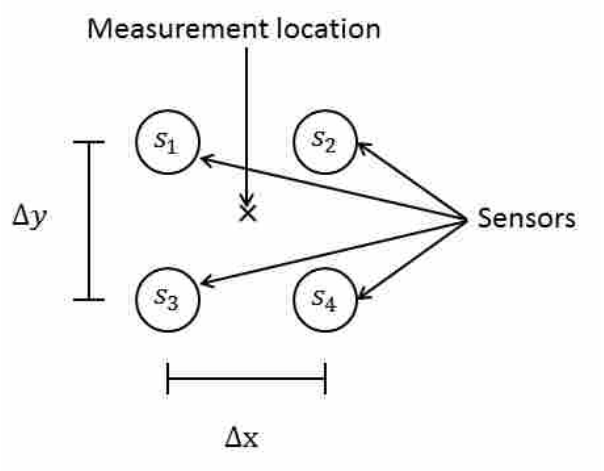

Figure 2-2: Schematic of Accelerometer Spacing used to Measure WSSG

$$w \approx \frac{s_1 + s_2 + s_3 + s_4}{4} \tag{2-1}$$

$$\frac{\partial w}{\partial x} \approx \frac{s_2 - s_1 + s_4 - s_3}{2\Delta x} \tag{2-2}$$

$$\frac{\partial w}{\partial y} \approx \frac{s_1 - s_3 + s_2 - s_4}{2\Delta y} \tag{2-3}$$

$$\frac{\partial^2 w}{\partial x \partial y} \approx \frac{s_2 - s_1 + s_3 - s_4}{\Delta x \Delta y} \tag{2-4}$$

Each sensor s_i represents the instantaneous acceleration coming from each accelerometer, and Δx and Δy represent the x and y distance between the accerometers respectively. Chapra and Canale[18] note that these equations are approximations derived from the Taylor series expansion and contain truncation error. The central difference method has a truncation error of the order of (Δx^2) which means the larger the distance between the sensors, the more truncation error will exist. Thus the accelerometers should be placed close to each other to minimize the effects from truncation error.

However, truncation error is not the only source of error in the tests; the random noise levels within the signals must also be taken into consideration. Generally, random noise can

cause a significant problem if the noise levels are within one order of magnitude of the measurements, but because several of the WSSG terms are formed by subtracting half of the readings from each other, the noise could have a significant effect if it is within one order of magnitude of the *difference* between two readings. This means the spacing between accelerometers should be increased in order to maximize the differences between the two accelerometer readings.

The optimal distance between the accelerometers is thus influenced by two opposing influences. Finite-differencing has less truncation error when the measurement points are closer, but random noise is less of a factor when the measurement points are farther apart. It was thus necessary to strike a balance between these effects and create an optimization routine which would determine the best spacing between the accelerometers based on expected random noise levels.

A simulation was designed to calculate WSSG on a flat plate using the finite difference method instead of taking the analytical derivatives (as had been done with previous simulations). This simulation calculated the transverse accelerations at a grid of points on a plate and then used equations 2-1 through 2-4 to calculate the three spatial derivatives at the center of the four points. WSSG was then calculated from these derivative terms and the finite difference WSSG ($WSSG_{FD}$) was compared to the analytical WSSG ($WSSG_A$) calculated from the previous simulations. In order to simulate noise in the accelerometer readings, random noise was added to the transverse accelerations at each point in the $WSSG_{FD}$. The magnitude of this noise was directly correlated to the measured noise levels in the actual accelerometers used to run the tests. This was done by measuring the signal-to-noise ratio of the actual data and then adding random

noise to the simulation using MATLAB®'s randn function until the same signal-to-noise ratio was attained in the simulation.

The optimization routine was then run to determine the best spacing of the accelerometers. The objective function used in the optimization routine was the average squared difference between $WSSG_{FD}$ and $WSSG_A$ across the face of the entire plate, shown in Eq. 2-5.

$$Average\ Diff = mean(WSSG_{FD} - WSSG_A)^2 \tag{2-5}$$

This routine was then repeated for each frequency of interest to see how the optimum changes with frequency. It is important to note that the optimal spacing for the accelerometers is highly dependent upon the individual accelerometers and system used. Some systems may have more noise than others, and so a new optimization routine should be run each time the system is changed.

A plot showing $Average\ Diff$ as a function of frequency and accelerometer spacing is given in Fig. 2-3. This plot was based on the expected noise levels within the experimental setup. It was discovered that the optimal spacing for the accelerometers is dependent upon the frequency of the excitation force and the resonance frequencies of the plate. When the plate was excited at a low frequency, away from the resonance frequencies, the plate did not vibrate with very high amplitudes. This meant that two closely spaced accelerometers were reading nearly the same value, and so any noise in the system had a large effect on the WSSG calculation. This is shown in Fig. 2-3 in the frequency range from 50 to 80 Hz, where the average squared error has extremely high values when accelerometer spacing is small. The accelerometers needed to be spread farther apart in order for them to read significantly different values.

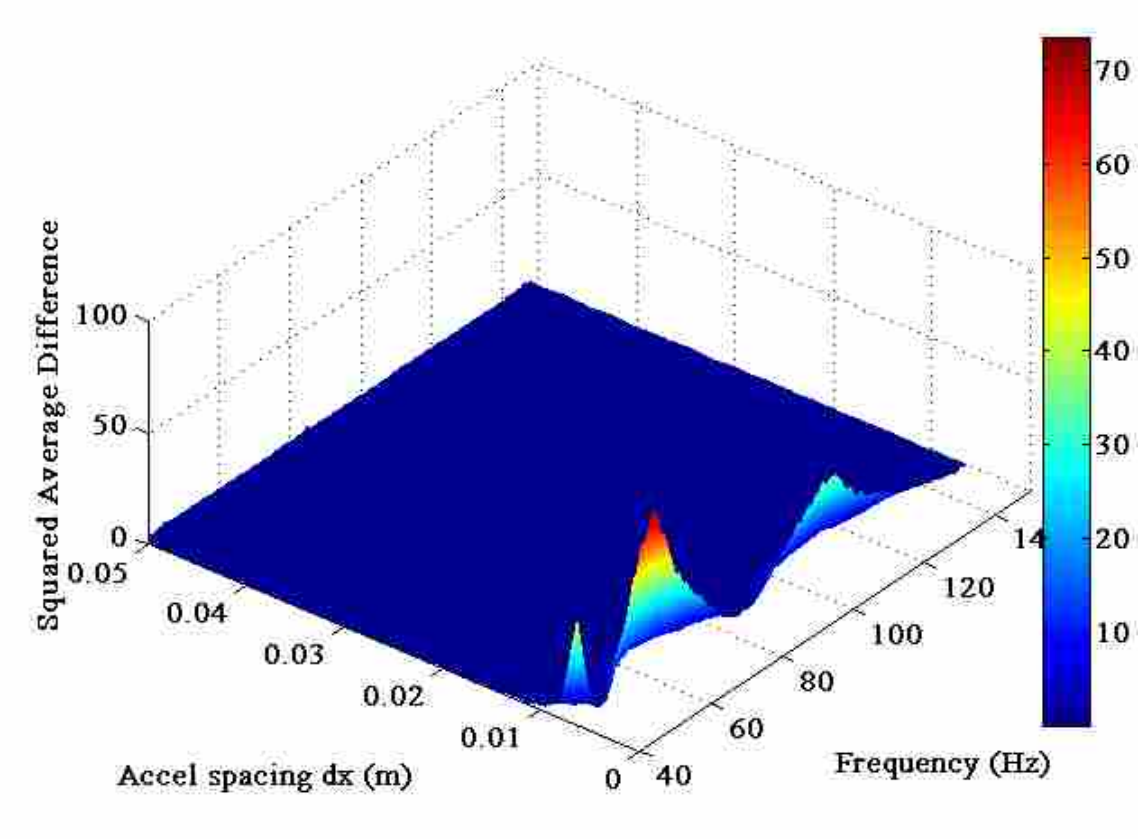

Figure 2-3: *Average Diff* as a Function of Frequency and Accelerometer Spacing

Conversely, when a natural frequency was approached, the plate would vibrate with higher amplitudes and so two closely spaced accelerometers did read significantly different values and the calculated WSSG approximation was closer to the analytical value. The accelerometers could thus be placed closer together before noise became a significant factor. This is seen in Fig. 2-3 near 47 and 87 Hz where the 1-1 and 1-2 structural modes are located. The average squared errors at these frequencies are much lower than at the off resonance frequencies.

If the frequency to be attenuated is known, a specific optimal spacing can be estimated. If a range of frequencies are to be attenuated, then an average must be made over the range of interest. This is what was done for the experimental tests shown in this thesis. It was determined

that the optimal spacing for the accelerometers based on the expected noise levels in the authors experimental setup was approximately 0.0243 m. This value is close to the standard English inch, (0.0254 m) and so a value of 0.0254 was chosen as the spacing to be used in all experimental tests.

The accelerometers were mounted to the vibrating plate by gluing nuts to the plate at a specific location and screwing the accelerometers into the nuts. An aluminum jig was created with nut-sized holes exactly 0.0254 m apart from each other in the configuration shown in Fig. 2-2. The nuts were placed on the jig and then glued to the plate while the jig held them exactly 0.0254 m apart. This was done so that the accelerometers could be placed at exactly the same distance apart for all test configurations.

Another possible source of error in the estimation of WSSG was the phase and magnitude differences between the individual accerometers. This was tested by attaching all four accelerometers close together on a large, flat, stiff shaker. The shaker was excited with a simple sine wave at several frequencies and the accelerometer time data was recorded using a Bruel and Kjaer pulse system. An SLDV simultaneously scanned the surface of the shaker in order to ensure the shaker maintained rigid piston-like motion (so that the actual phases of the accelerometers would be in synch).

The accelerometer signals were plotted together in order to measure the phase and amplitude differences between the accelerometers. It was initially determined that there was indeed an amplitude mismatch between the accelerometers. This was corrected by calibrating the accelerometer sensitivities and performing the test again. With the correct accelerometer sensitivities the difference between the magnitude and phases of the accelerometers were determined to be negligible. The differences between the magnitudes were approximately one

order of magnitude below the amplitude of the estimated random noise in the experimental setup. This means the random noise has a much greater impact on WSSG than amplitude differences in the accelerometers.

The difference in the phases of the accelerometers was also determined to be negligible.

2.3 **Degenerate Modes**

During experimental tests using a scanning laser Doppler vibrometer (SLDV), it was determined that there are cases when two structural modes shapes occur at the same frequency. These are called degenerate modes. Common sources of degenerate modes are plates whose x and y side lengths are integer multiples of each other. Because the frequencies of these two modes are the same, the two individual mode shapes will superimpose on top of each other and cause distortions in their structural modes. This distorted mode shape is often quite different in appearance from normal modes. It was discovered during experimental tests that controlling a degenerate mode with WSSG often did not result in significant radiated sound power attenuation and it became necessary to perform more simulations to better understand the phenomenon.

New simulations were created which calculated the velocities of a vibrating simply supported plate which contained several degenerate modes. Sound power levels were calculated using the method of elementary radiatiors[2] when the plate was being excited with a single point force and then compared to sound power levels when WSSG was being minimized at a single point by a control force. These plots demonstrated that the performance of WSSG as a sound power minimization parameter suffered whenever a degenerate mode was present. Often, little or no attenuation was achieved and even when attenuation was achieved, it was not as high as non-degenerate modes. An example of one of these plots is shown in Fig. 2-4. In this figure the degenerate modes are located at 19, 38, 49 and 64 Hz.

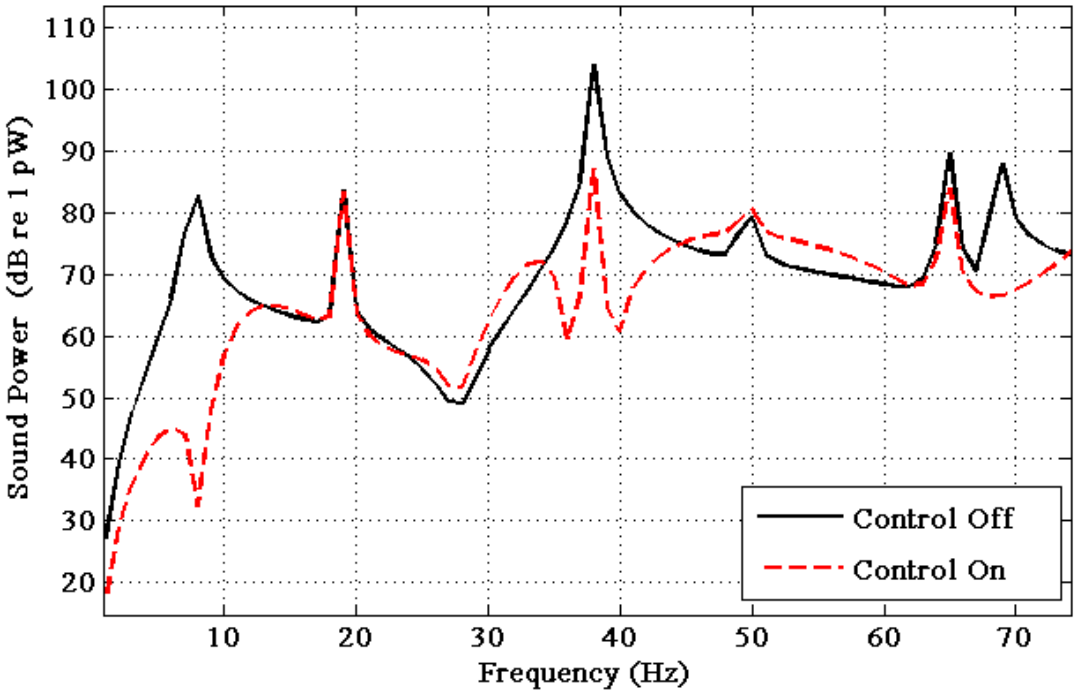

Figure 2-4: Simulated Sound Power Radiated from a Plate with Degenerate Modes for a Single Control Force

These results were analyzed in an attempt to achieve control at these frequencies while still using WSSG as the minimization quantity. It was determined that degenerate modes simulate an additional degree of freedom to the plate and so it was assumed that adding an additional degree of control to the plate would help. This was done by adding a second control force to the plate and coding the simulations to minimize WSSG by controlling both control forces simultaneously. Figure 2-5 shows the sound power radiated when two shakers are used to control the simply supported plate.

This figure shows that adding a second control force does allow WSSG to effectively control the plate when degenerate modes are present. The degenerate modes at 19, 38 and 64 Hz were attenuated significantly. The 2-3 and 3-2 modes located at 49 Hz were not attenuated significantly, but it did perform better than it did when only one control force was present. When one control force was present, WSSG amplified the sound power at that location, but when two

control forces were present, it brought the peak down to the level of the surrounding frequencies. Results similar to this were observed for several different control and plate configurations. This led the researchers to believe that controlling a degenerate mode is possible if an additional control force is added.

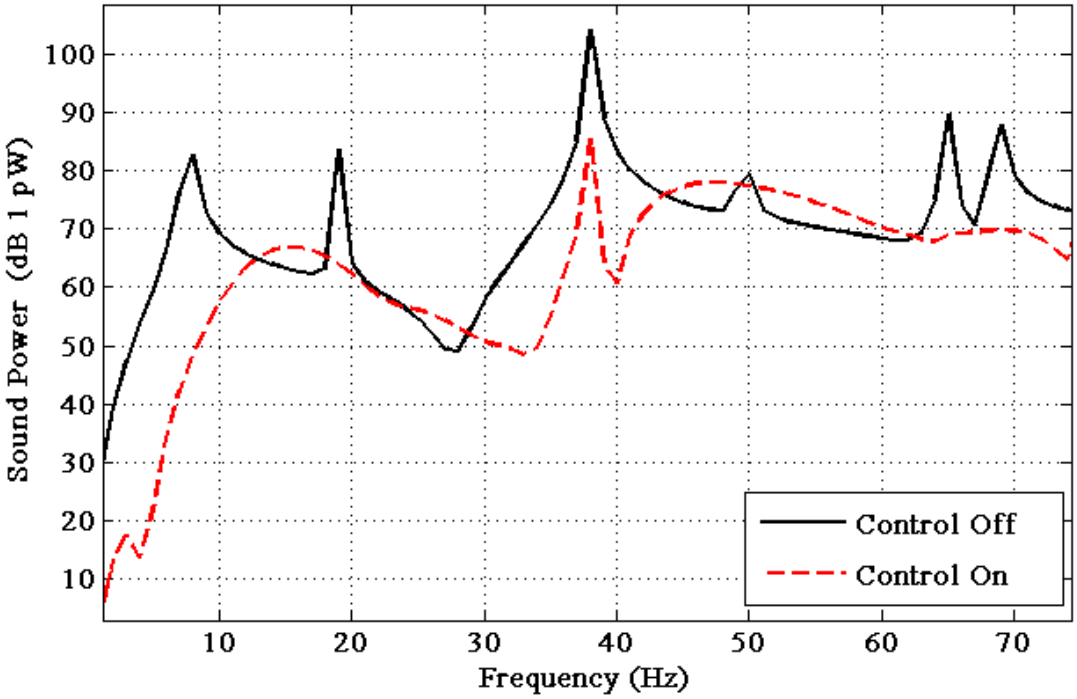

Figure 2-5: Simulated Sound Power Radiated from a Plate with Degenerate Modes for two Control Forces

2.4 Square Plates

Square plates represent a special case of the degenerate mode analysis. As was explained in the previous section, degenerate modes occur most often when the side lengths of a plate are integer multiples of each other. When the side lengths are *equal* to each other, then degenerate modes will occur for every case except where $m = n$. This means nearly every mode on the plate will be a degenerate mode and that the overall attenuation for a square plate will be very small, if not negative.

Figure 2-6 shows an example of a control plot for a square plate. The side lengths of this plate are both 0.754 m and the disturbance force (F_d), control force (F_c) and sensor (S) are located at $F_d = (0.397, 0.625)$ m, $F_c = (0.124, 0.467)$ m and $S = (0.146, 0.289)$ m. In this simulation there is an overall attenuation of -0.9 dB, which means that there is actually an overall amplification of the noise.

Adding a second control force does help to control the plate and an overall sound attenuation is achieved. Figure 2-7 shows the control results when two control forces are used, with the additional control force (F_{c_2}) placed at $F_{C_2} = (0.320\ 0.133)$ m. This plot has an overall attenuation of 7.1 dB and represents a significant improvement over the single control force plot. These results suggest that a second control force should always be used when a square plate is being controlled.

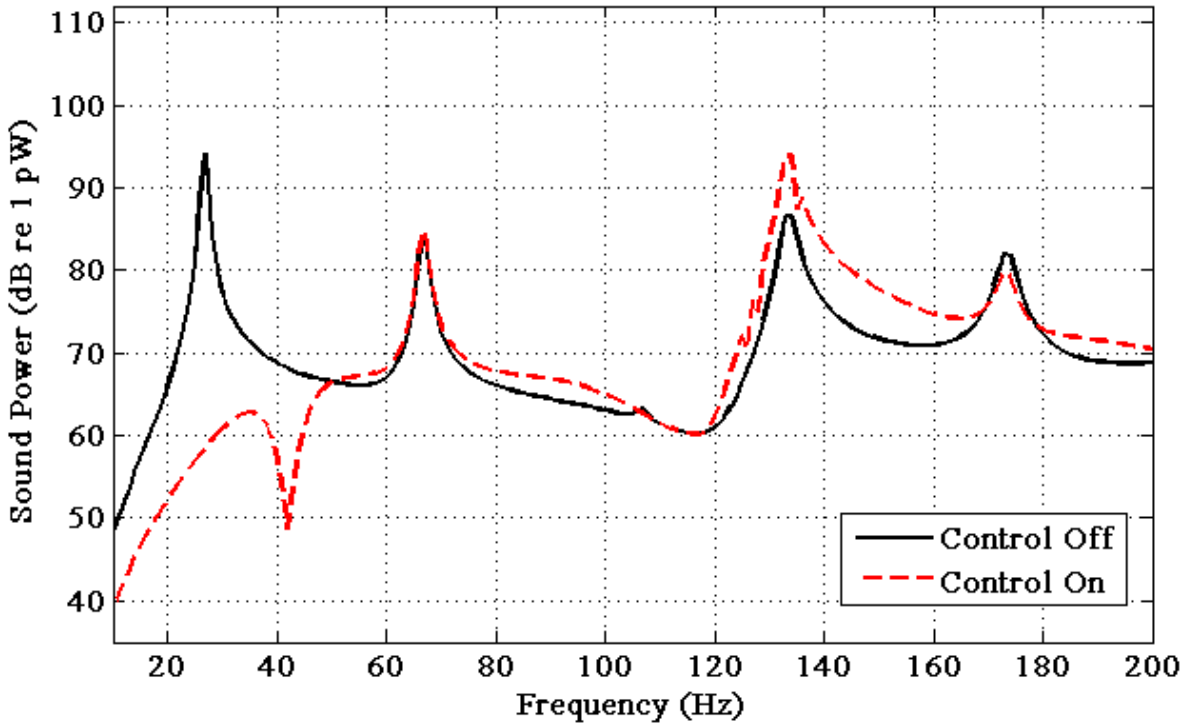

Figure 2-6: Sound Power for Control of a Square Simply Supported Plate with One Control Force.

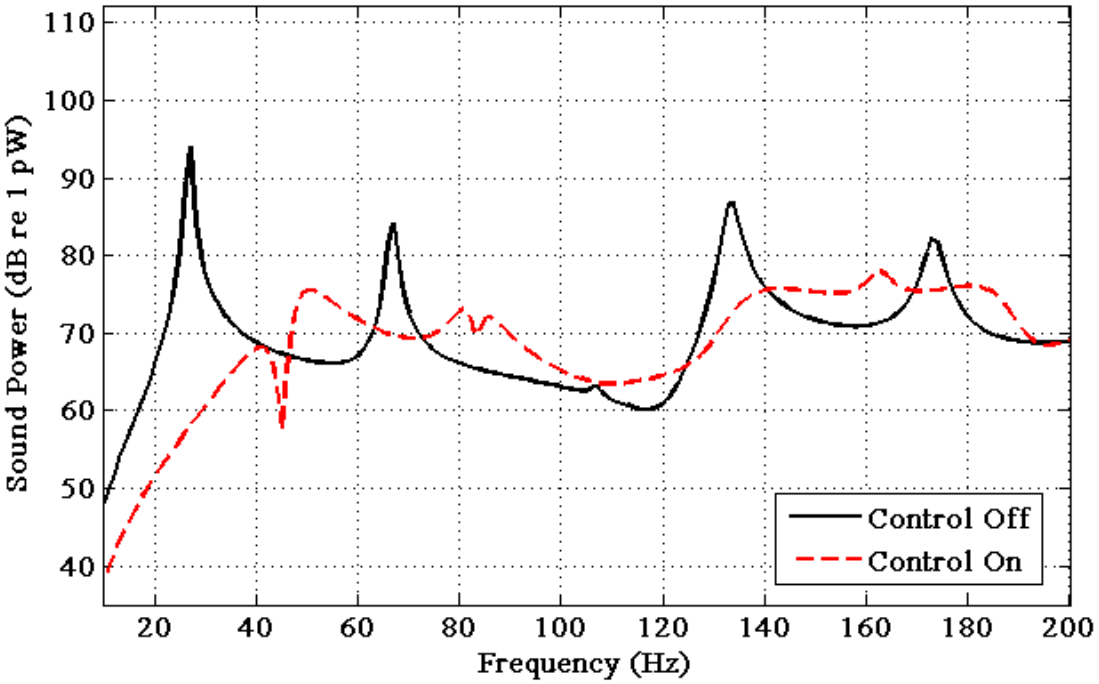

Figure 2-7: Sound Power for Control of a Square Simply Supported Plate with Two Control Forces.

2.5 Analytical Conclusions

The analyses presented in this chapter represent important advances of the WSSG theory which were necessary before experimental results could be measured. It was determined that the weights used in the WSSG formulation are highly resilient and that there was little difference between using an average over several modes and the frequency specific weights. The noise levels in the system were modeled in computer simulations and an optimal sensor spacing was determined to minimize the effects of noise in the measurement. Degenerate modes were shown to negatively affect the control results of WSSG but it was shown that adding a second control force could significantly boost the attenuation levels. This was shown to be the case for square plates as well, which have significantly more degenerate modes than non-degenerate modes.

3 EXPERIMENTAL RESULTS FOR SIMPLY SUPPORTED PLATES

This chapter details the experimental work using WSSG as the minimization quantity in the acoustic control of a vibrating simply supported plate. The setup of the experiment is shown, followed by plots of WSSG as measured across the surface of the plate for several modes. This was done to validate the experimental uniformity of WSSG and to ensure it matches the theory developed by Fisher *et al.*[15] Control plots are then shown for both one and two control force situations and these are compared to the computer simulations with the same configurations. The results are discussed.

3.1 Experimental Setup

A simply supported plate was assembled using 6061-T6 rolled aluminum; a list of the properties is given in Table 1-2. The simply supported boundary conditions were created by suspending the plate in a stiff frame with set screws, spaced 1.6 cm apart, whose points touch the four sides of the plate as shown in Fig. 3-1. Care was taken to ensure rotation was still possible at the edges. This was done by milling a groove into the side edge of the plate at an angle of 100 degrees. The set screws came to a point at an angle of 90 degrees. The groove thus allowed the screws to self-center themselves in the middle of the edge, while still allowing rotation to occur at the edges. Spatially dense velocity measurements across the entire plate were made with an SLDV to ensure the simply supported boundary conditions were met (that rotation was possible but translation was not).

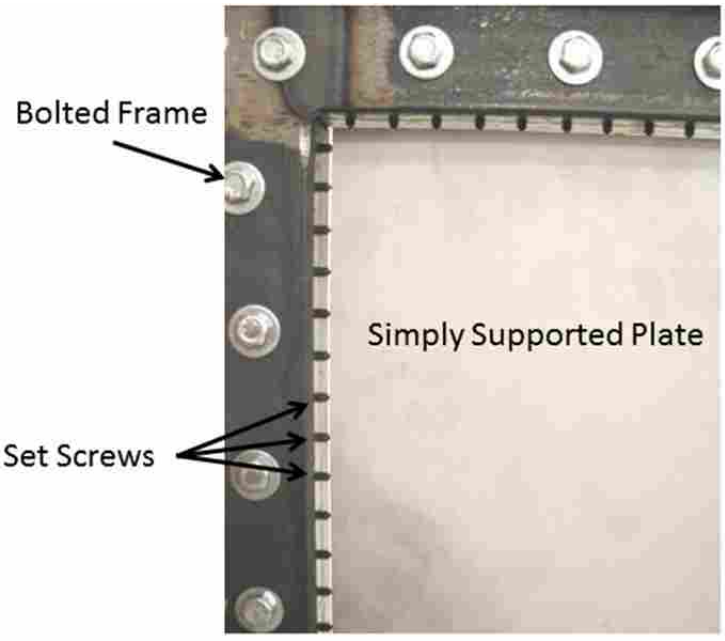

Figure 3-1: The Simply Supported Boundary Conditions

The plate was excited with a Labworks ET-126 shaker attached to a signal generator and controlled with a Bruel and Kjaer type 4809 Vibration Exciter. These shakers were suspended from a stiff frame and attached to the plate by gluing the individual stingers to the back side of the plate. WSSG was measured at a point using four accelerometers placed 0.0254 m apart in the configuration shown in Fig. 2-2. The accelerometer signals were channeled through a filter and into a DSP controller which calculated WSSG using Eqs. 2-1 through 2-4. Control was achieved using a modified Filtered X LMS algorithm in the DSP controller which optimized the phase and amplitude of the control shaker to minimize WSSG. Fisher[10] details the update made to the F-X LMS algorithm. The SLDV was used to measure the velocity at an array of points on the plate and then sound power was calculated using the method of elementary radiators[2]. A schematic of the experimental set up is shown in Fig. 3-2.

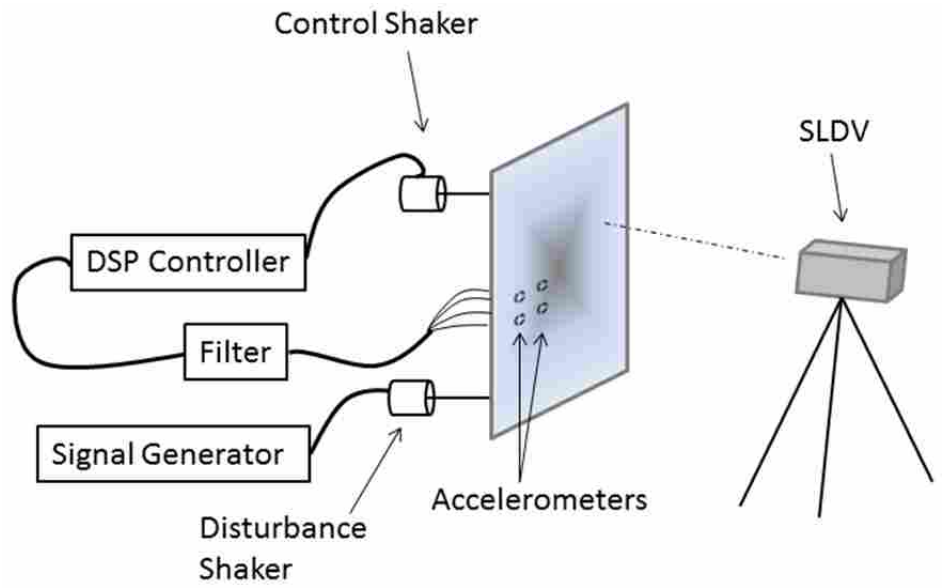

Figure 3-2: Schematic of the Experimental Setup.

The simply supported plate was then placed in a window between two large acoustic reverberation chambers. This provided a baffle between the two sides of the plate and isolated the plate from any outside vibrations or noises. The two reverberation chambers had dimensions of 4.96m X 5.89m X 6.98m and 5.70m X 2.50m X 4.30m. These chambers had multiple axial, tangential and oblique room modes whose resonances fell within the frequency range of the WSSG tests, and so it is possible these could have caused additional loading on the plate. No attempt to analyze the room mode effects on the vibrating plate were made in this thesis.

3.2 Experimental Validation of WSSG Theory

Before the plate was set up in the manner shown in Fig. 3-2, it was necessary to validate the uniformity of WSSG and ensure that it matched theory. This was done by placing a single shaker in the lower right corner of the plate and measuring WSSG across the face of the plate for several of the modes. Only one shaker was used in order to have the least amount of distortion in the structural modes. The four WSSG terms were calculated by applying Eqs. 2-1 through 2-4 to

spatially dense SLDV measurements. The individual WSSG terms for the 1-1 mode are shown in Figure 3-3.

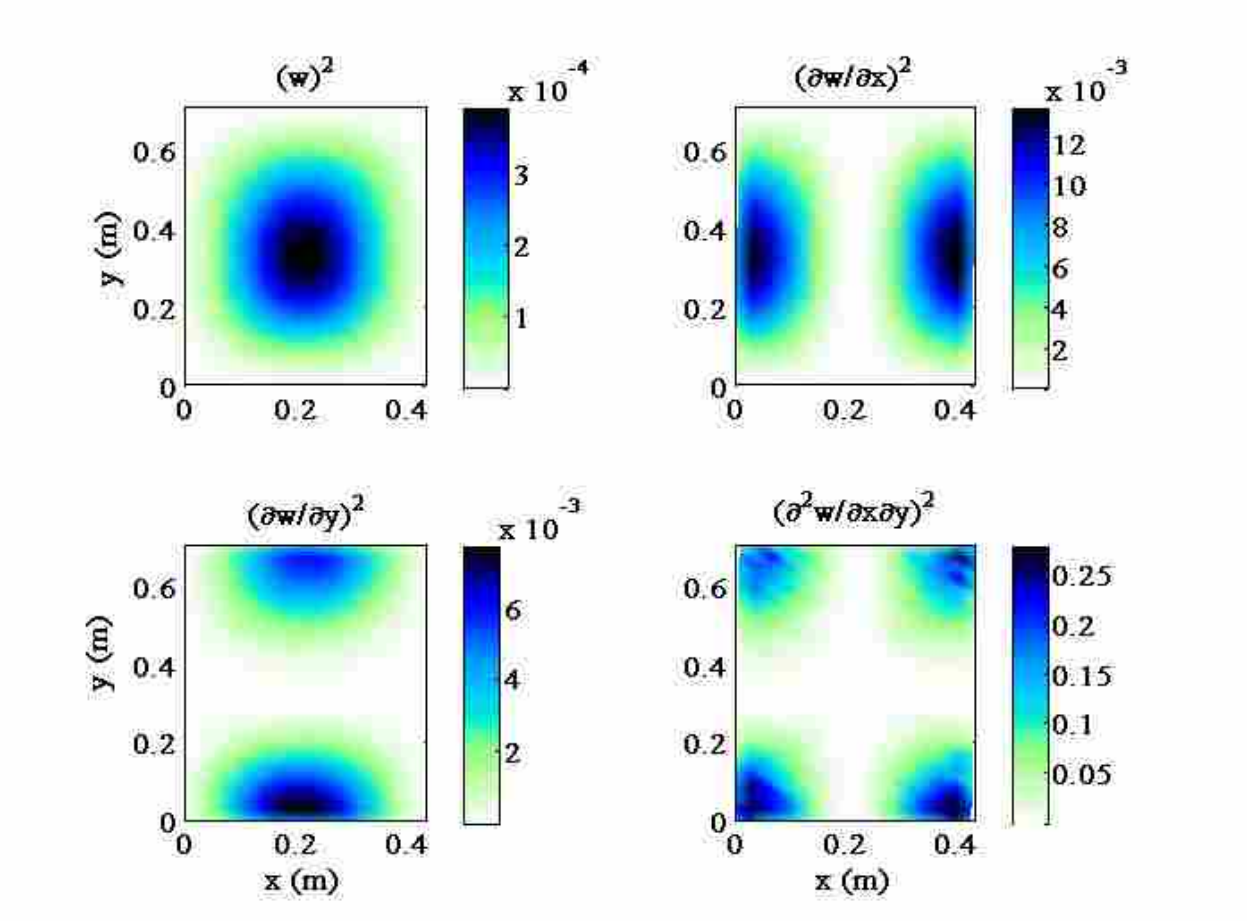

Figure 3-3: Plots of the Four WSSG Terms of the 1-1 Mode

If the magnitudes of these four terms were normalized then they would match the analytical plots shown in Fig. 1-2. When these four terms are combined using the proper weights, a nearly uniform quantity is obtained. Figure 3-4 shows the combined WSSG field for the 1-1 mode. This is a close match to the analytical plots, but it is not perfect. The higher values at the lower part of the plate are due to the placement of the shaker at the bottom of the plate. This caused the first structural mode to skew slightly downward and higher derivatives were measured at the lower portion of the plate, as evidenced by the $\left(\frac{\partial w}{\partial y}\right)^2$ plot in Fig. 3-3.

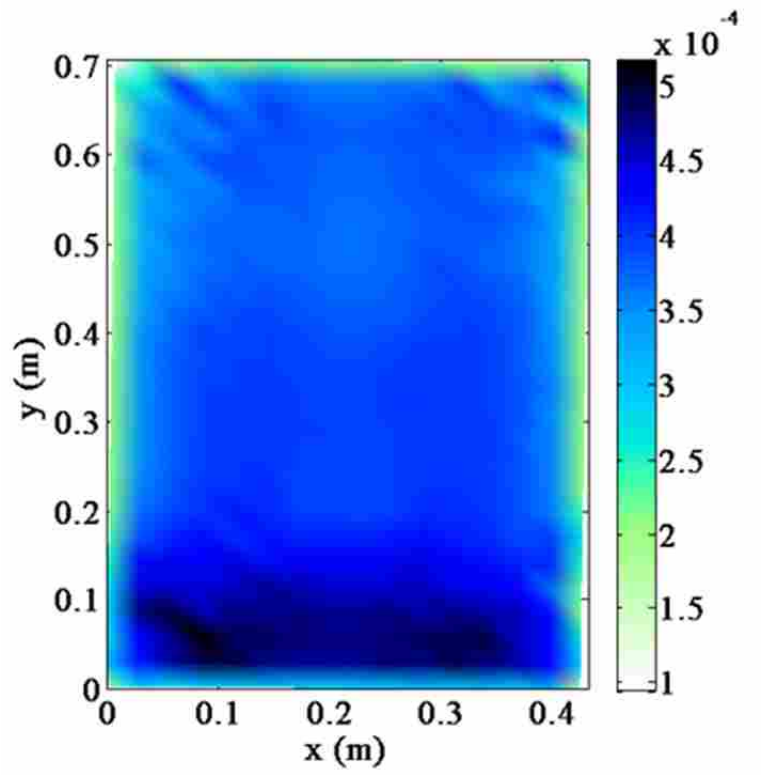

Figure 3-4: Total WSSG Field from the 1-1 Mode, with Frequency Specific Weights

Figure 3-5 shows plots of the combined WSSG fields for the next four modes when the ideal mode-specific weights are used. These plots show that experimentally measured WSSG may not be perfectly uniform for higher modes. The non-uniformities on each of these plots can be traced to the non-uniform amplitudes of the anti-nodes. For example, on the fourth mode (the 2-2 mode), the shaker is located in the lower right corner of the plate, much closer to the lower right anti-node than the lower left. The SLDV scans showed that this caused the right anti-node to have a higher amplitude than the left anti-node. Perfect uniformity was thus not obtained. However, the amplitude of the left anti-node is still 90% of the right anti-node, and so placing the WSSG sensor in either quadrant will still cause significant sound attenuation of the mode.

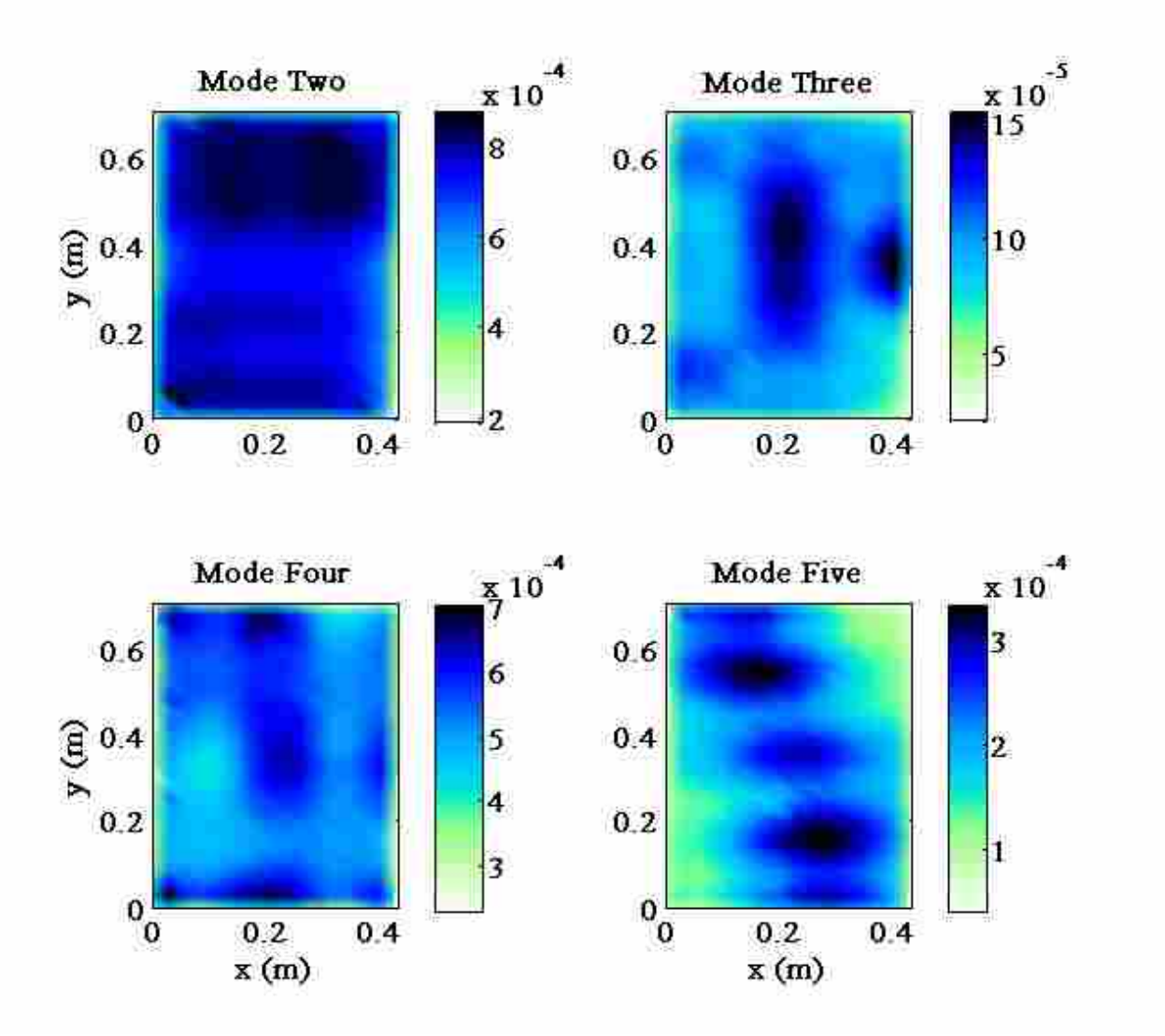

Figure 3-5: Plots of the Total WSSG Field for Modes Two through Five

Modes three and five both had larger variations in the amplitudes of each anti-node and so were not nearly as uniform. This is because the third mode is actually a degenerate mode with the 2-1 mode and the 1-3 modes superimposing on each other. Mode five is close to being degenerate and its 1-4 mode is greatly influenced by the nearby 2-3 mode. Similar results were noticed for higher modes. Whenever a resonant frequency was isolated (far away from any other natural frequency) a nearly uniform WSSG field was calculated, but when resonant frequencies were close to each other, then the WSSG field was less uniform.

3.3 Experimentally Measured Sound Power Results

The plate was set up in its first configuration and the computer model updated so that the sensor and shaker positions would match the experimental configuration. This allowed for a comparison between analytical models and experimental data to be made. Several configurations were tested, each with different sensor and shaker positions. However, only four tests, representing two different configurations, will be shown in this thesis. The shaker and sensor positions for each configuration are shown in Fig. 3-6, with the exact locations given in Table 3-1.

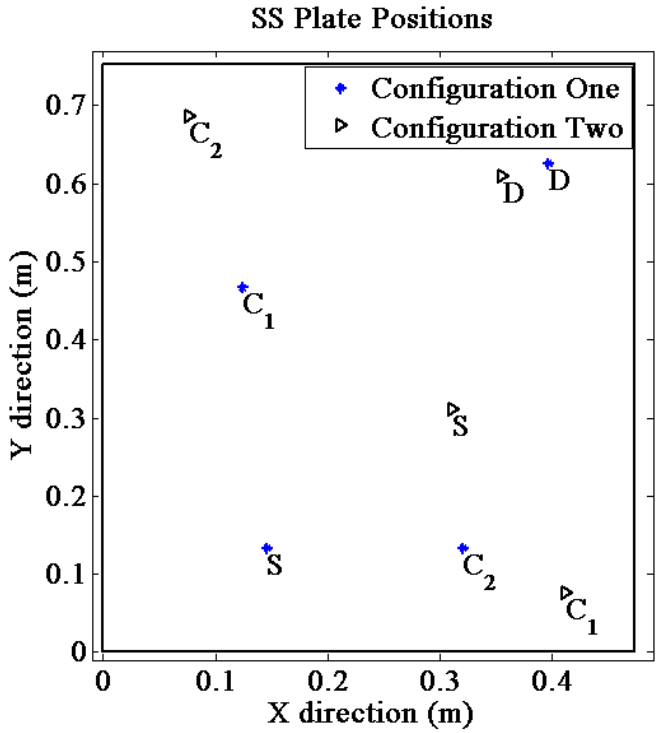

Figure 3-6: Experimental Simply Supported Plate Configurations

In Fig. 3-6, D is the disturbance force location, C1 is first control shaker location, C2 is the second control shaker location (if applicable) and S is the location of the center of the four accelerometers used to measure WSSG.

Table 3-1: Actuator and Sensor Locations for the Simply Supported Plate Experiments

Actuator/Sensor	Configuration one location (x, y)	Configuration two location (x, y)
Disturbance	$(0.397, 0.625)$	$(0.406, 0.686)$
Controller one	$(0.124, 0.467$	$(0.413, 0.076)$
Sensor	$(0.146, 0.133)$	$(0.311, 0.311)$
Controller two (if applicable)	$(0.321, 0.1334)$	$(0.076, 0.686)$

It was noted that the two shakers used in the experimental results were relatively heavy (well over 5 kgs) and thus provided an additional source of stiffness and mass loading to the plate. This mass loading and additional stiffness from the shakers was not modeled in the computer simulations but caused the natural frequencies of the experimental plate to shift from the values computed by the model. Therefore the simulated and experimental results were not plotted on the same graph. However, a comparison can still be made between the results by comparing the frequencies with the same mode shapes. The shakers also changed the damping coefficient of the plate. With the shakers attached to the plate an experimental damping coefficient was measured to be 2% ($\eta = 0.02$) using the method of logarithmic decrement. This is higher than the damping coefficient measured without the shakers attached.

Figures 3-7 and 3-8 show the computer and experimental sound power plots, respectively, for configuration one with a single control force. The analytical model was made with a frequency increment of 1 Hz, while the experimental test was made with a frequency increment of 5 Hz. Additional experimental data points were also measured at each of the resonance frequencies in order to measure the peaks.

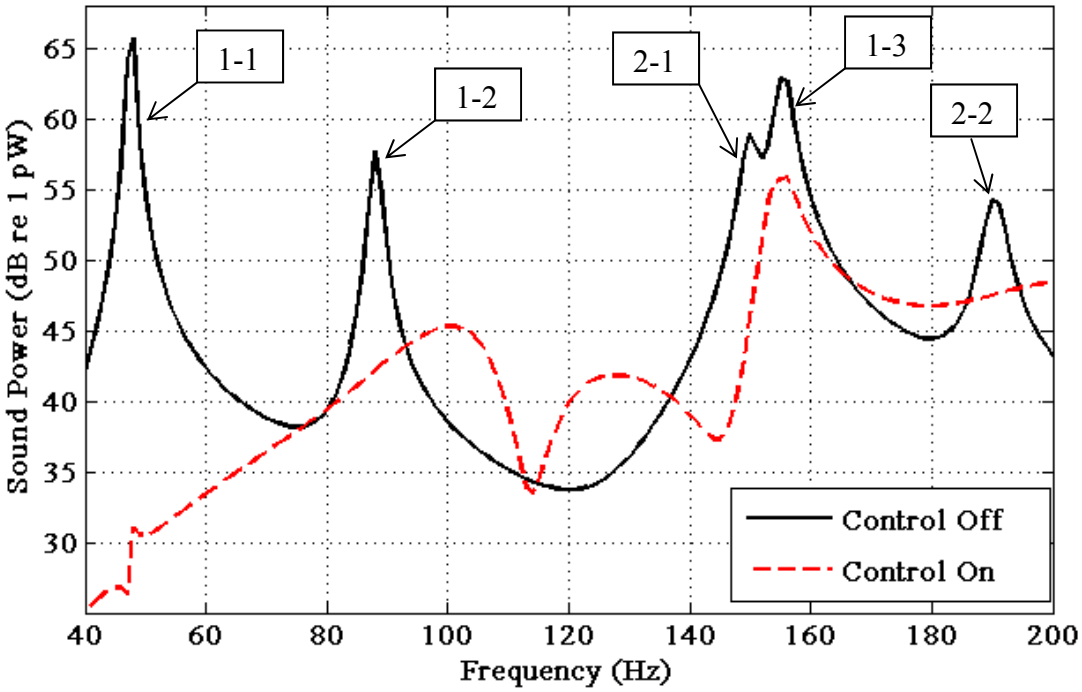

Figure 3-7: Computer Simulation of Sound Power Results for Control of WSSG in Configuration One with One Control Force

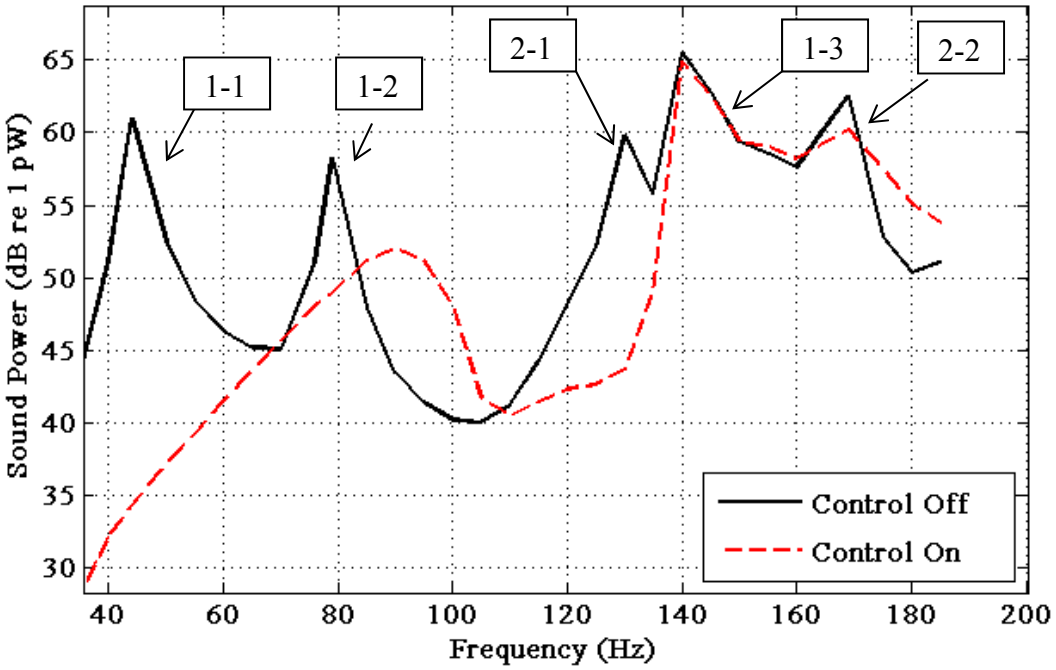

Figure 3-8: Experimental Sound Power Results for Control of WSSG in Configuration One with One Control Force

These plots demonstrate several important features about the use of WSSG in an experimental set up. First is that the experimental plots generally show the same trends and shapes as the computer simulations, but the amplitudes of the attenuations are generally smaller. Table 3-2 contains the attenuation levels for each mode, as well as the overall sound power attenuation. This table shows that both plots have significant attenuation levels at the 1-1 mode, 1-2 mode and 2-1 mode, with smaller attenuation levels at the 1-3 and 2-2 modes. The largest discrepancy between the two plots comes at the 1-3 and 2-2 modes, where the computer simulations predict 7.2 dB and 6.8 dB of attenuation, respectively, but the experimental tests only attain only 0.7 dB and 2.3 dB of attenuation, respectively.

Table 3-2: Attenuation Levels for One Control Shaker, Simply Supported Configuration One.

	Configuration One	
Mode	Simulation (dB)	Experimental (dB)
1-1 Mode	37.9	26.7
1-2 Mode	15.6	9.4
2-1 Mode	14.5	19.2
1-3 Mode	7.2	0.7
2-2 Mode	6.8	2.3
Overall attenuation	6.1	1.4

Figures 3-7 and 3-8 both show an amplification of radiated sound power in between the 1-2 and 2-1 modes. The maximum amplification levels for the simulated and experimental plots are 7.8 dB and 9.8 dB, respectively. While this may appear to be a large level of amplification, these amplifications occur in between modes, where the uncontrolled power levels are much lower. Thus the amplified levels are still 15 to 20 dB below the levels radiated by the resonant frequencies. These amplified levels have little effect on the overall attenuation levels attained.

The computer simulations predict an overall attenuation of 6.1 dB, while the experimental plots show an overall attenuation of only 1.4 dB. The low overall attenuation of the experimental data is chiefly due to the fact that the experimental results show very minimal sound attenuation for the 1-3 mode, which has the highest sound power level. Significant control is achieved elsewhere, but the mode which outputs the most sound power is not well controlled.

If the total sound power levels are calculated for just the first three modes (from 35 to 130 Hz) then 6.2 dB of attenuation is achieved in the experimental results. This represents a significant reduction in sound power levels over that frequency range.

One of the main reasons for the attenuation amplitude level differences between the computer models and the experimental plots may be noise. It was demonstrated in Section 2.2 that an optimal accelerometer spacing can be found to minimize the effects of noise in the system, but not to eliminate the effects completely. Even with the optimal accelerometer spacing, there was still an 8 to 9 % difference between $WSSG_{FD}$ (with noise) and $WSSG_A$ at the natural frequencies in the computer simulation. These differences were amplified when the plate was being forced at an off resonance frequency and often there was a 20% difference between $WSSG_{FD}$ and $WSSG_A$ in the simulations. Errors in the measured WSSG values make it difficult for the control algorithm to find the optimal values of the amplitude and phase for the control shaker, which will lessen the amount of control attained. This may account for the amplitude differences between the computer and experimental sound power plots.

Another possible reason for the differences is that the experimentally measured WSSG was not as uniform across the plate as the theory predicted for higher modes. This was mentioned in Section 3.2. This means it is possible the accelerometers may not have been located in the best position to measure the vibration of the plate.

Figures 3-9 and 3-10 show the computer and experimental plots (respectively) for configuration two with one control force and include the first seven modes instead of only five. These plots showed similar trends as in configuration one, but with one major difference; the natural frequencies shifted significantly between the 2-1 and 2-2 modes on the experimental plots. This frequency shift was shown to be a result of the added mass loading from the shakers. This was shown by measuring the frequency response of the plate twice; once with the heavy disturbance and control shakers attached in configuration two and once with a single (much lighter) LDS V203 shaker placed in the corner. The frequency response of the plate with LDS shaker closely matched the frequency response of the simulated plate. The frequency response of the plate with the disturbance and control shakers attached showed shifted frequencies. The only difference between the setup of the two measured experimental frequency responses was the shakers attached to the plate. This suggests the shakers were mass loading the plate, which caused the shifted frequencies.

Table 3-3: Attenuation Levels for One Control Shaker, Simply Supported Configuration Two.

	Configuration Two	
Mode	Simulation (dB)	Simulation (dB)
1-1 Mode	36.7	36.7
1-2 Mode	19.7	19.7
2-1 Mode	26.9	26.9
1-3 Mode	30.5	30.5
2-2 Mode	7.8	7.8
1-4 Mode	7.5	7.5
2-3 Mode	1.5	1.5
Overall attenuation	3.3	2.7

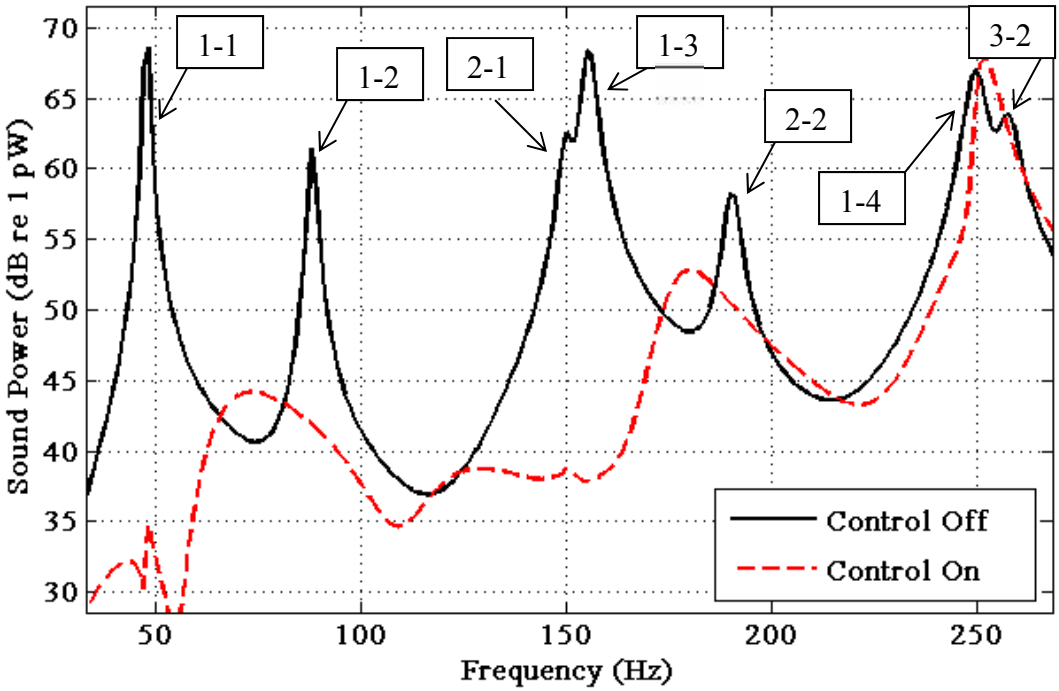

Figure 3-9: Computer Simulation of Sound Power Results for Control of WSSG in Configuration Two with One Control Force

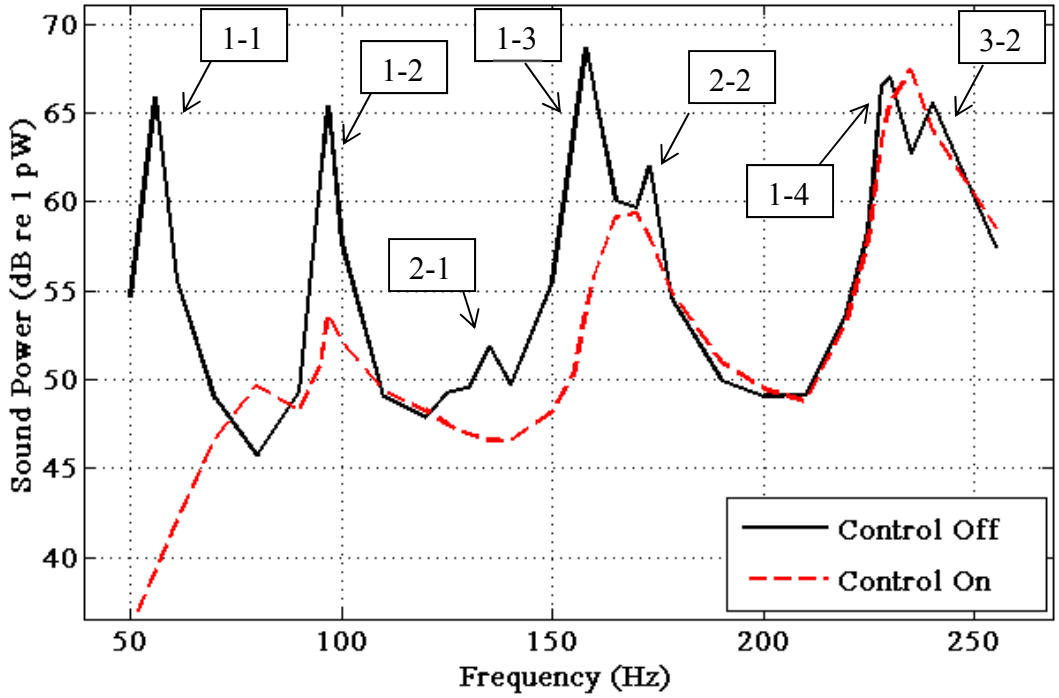

Figure 3-10: Experimental Sound Power Results for Control of WSSG in Configuration Two with One Control Force

The shifted frequencies of the experimental results make it difficult to do a direct comparison between the simulated and experimental data, but important insights can still be gained. Figures 3-9 and 3-10 both show significant attenuation at the first four modes and moderate attenuation at mode five (the 2-2 mode). Both also show minimal control at the 1-4 and 3-2 modes with amplification occurring between their peaks. As was the case in configuration one, the experimental plot showed much lower levels of attenuation, even though the same general trends were seen. Similarly, both plots had some frequencies which were amplified. The simulation predicted an overall attenuation of 3.3 dB attenuation, while the experimental plots showed an actual overall attenuation of 2.7 dB. Both plots achieve attenuation of the major source of radiated power, (the 1-3 mode) but both plots fail to achieve significant control on the sixth and seventh modes.

If overall attenuation levels are calculated for just the first five modes (from 50 to 210 Hz) then 6.5 dB of attenuation is achieved on the experimental plate. This is also a significant level of attenuation for that frequency range.

As was noted earlier, several of the natural frequencies where WSSG fails to cause significant attenuation are actually degenerate modes. Thus both configurations were run again with an additional control force added to the plate. The shaker added was an LDS V203 shaker. The results of these tests are shown in Figs. 3-11 through 3-14. Figures 3-11 and 3-12 show the computer and experimental plots (respectively) for configuration one and Figs. 3-13 and 3-14 show the computer and experimental plots (respectively) for configuration two.

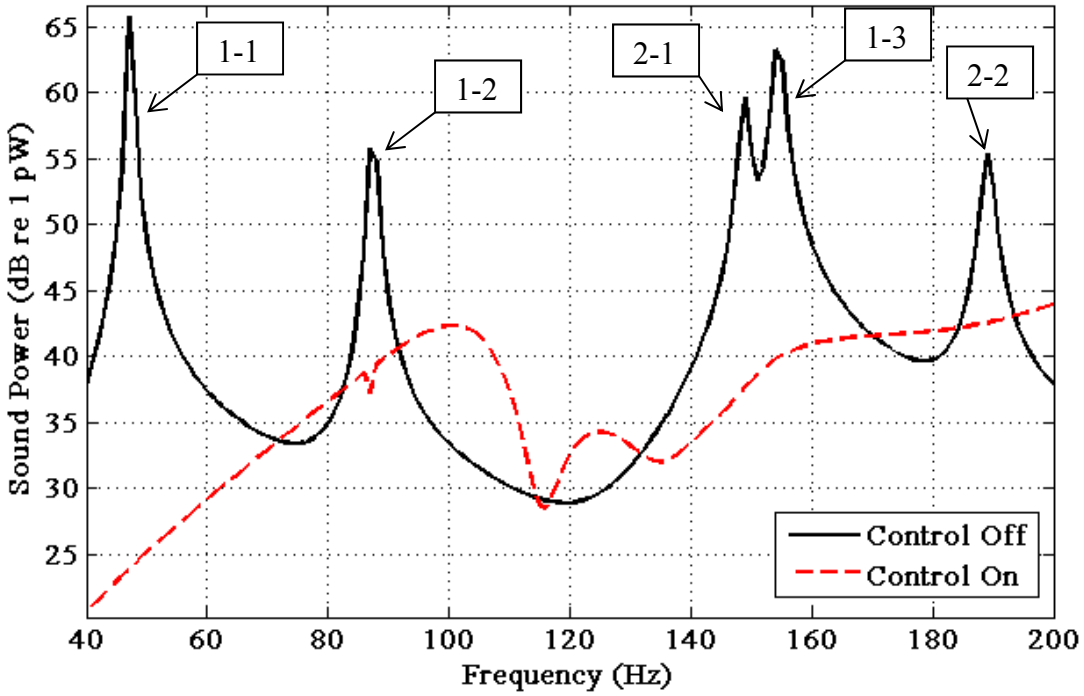

Figure 3-11: Computer Simulation of Sound Power Results for Control of WSSG in Configuration One with Two Control Forces

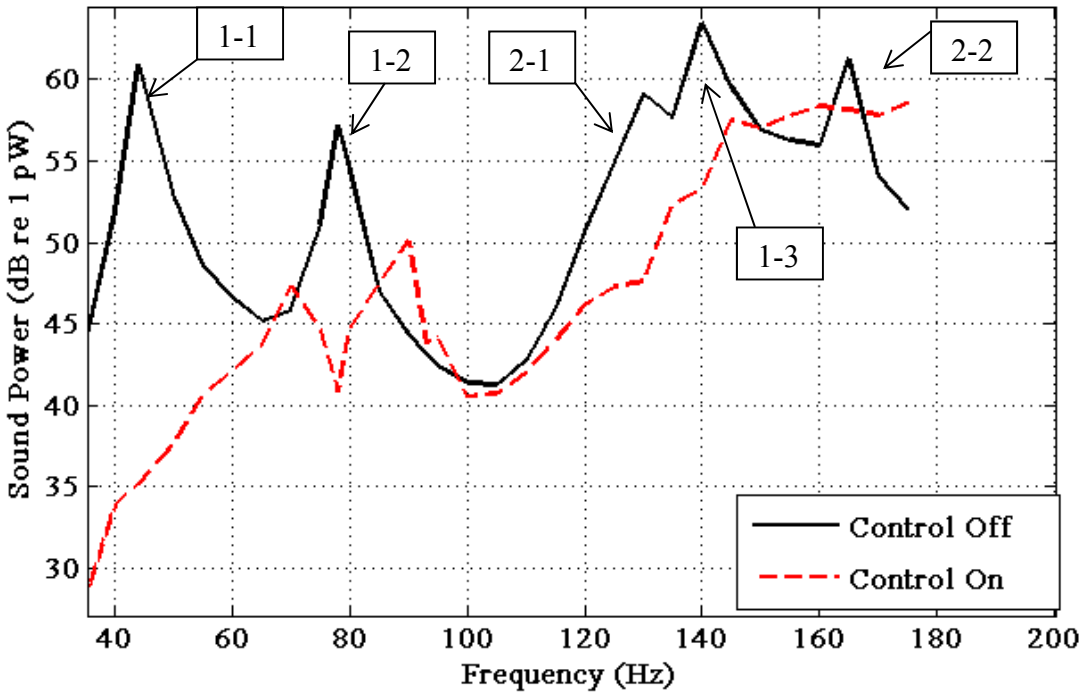

Figure 3-12: Experimental Sound Power Results for Control of WSSG in Configuration One with Two Control Forces

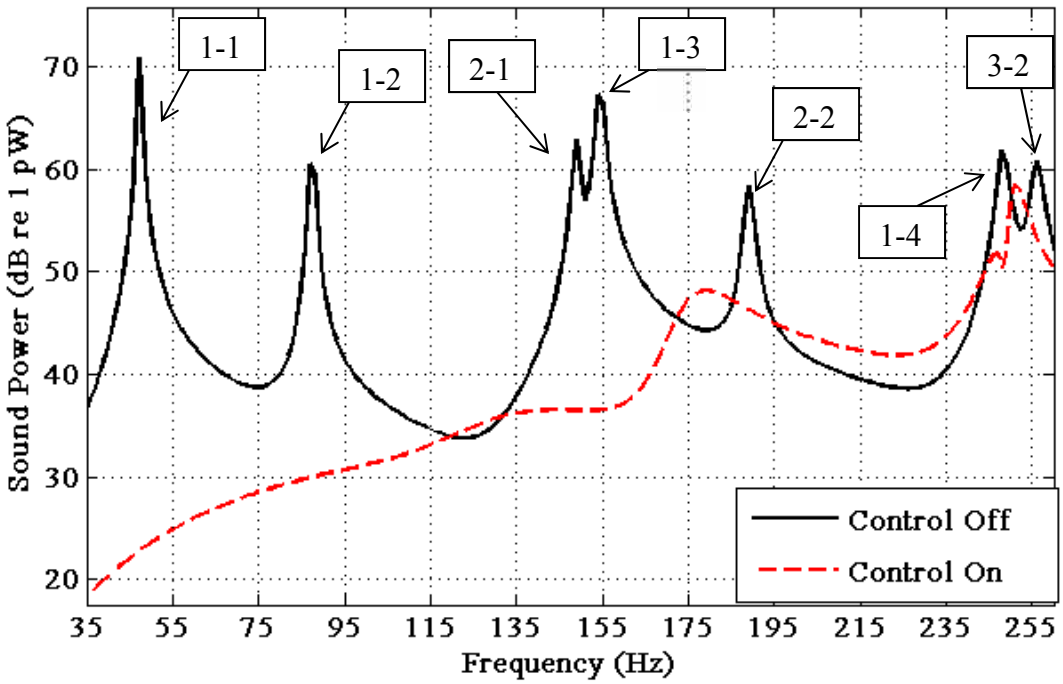

Figure 3-13: Computer Simulation of Sound Power Results for Control of WSSG in Configuration Two with Two Control Forces

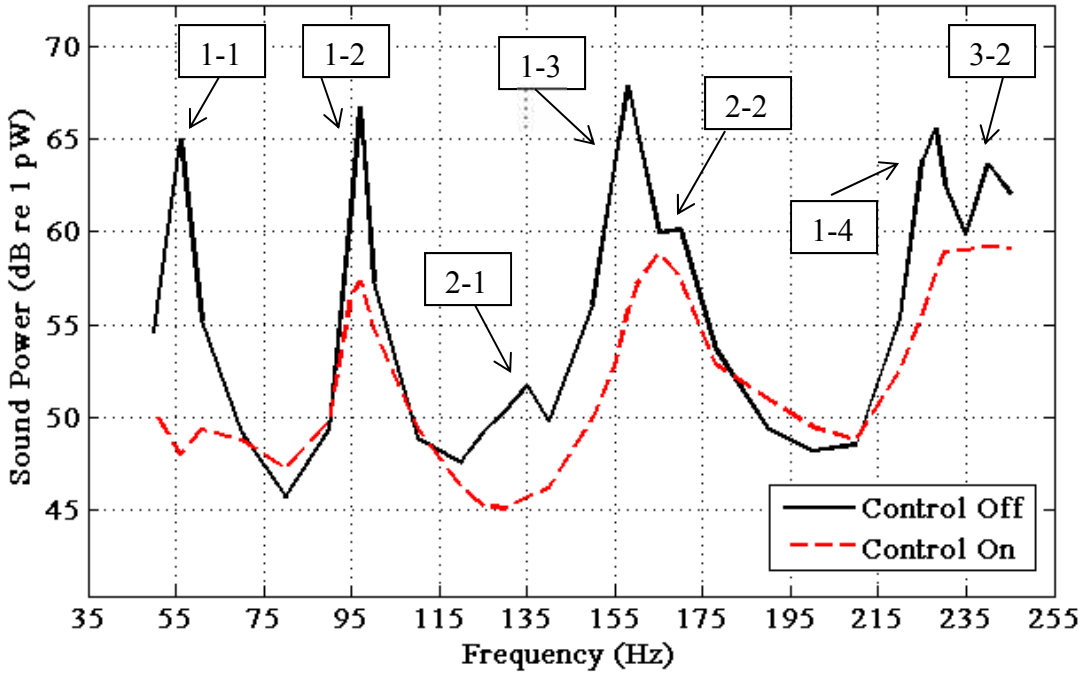

Figure 3-14: Experimental Sound Power Results for Control of WSSG in Configuration Two with Two Control Forces

These results once again show that the experimental results have the same general shapes and trends as the simulated results, but less attenuation. In configuration one, the overall attenuation increased by 5 dB in the simulated results, and by 1.9 dB in the experimental results. This increase was caused mainly by the added control achieved at the 1-3 mode, which was the largest contributor to total sound power radiated. The list of attenuation levels at each mode is presented in Table 3-4. The list further confirms the analysis presented in Section 2.3, which showed that adding a second control force significantly helps control degenerate modes.

Table 3-4: Attenuation Levels for Two Control Shakers for the Simply Supported Plate

	Configuration One		Configuration Two	
Mode	Simulation (dB)	Experimental (dB)	Simulation (dB)	Experimental (dB)
1-1 Mode	41.9	25.7	48.2	17.1
1-2 Mode	16.8	16.3	30.6	9.4
2-1 Mode	21.9	11.5	26.5	5.9
1-3 Mode	26.5	10.1	30.7	12.2
2-2 Mode	12.8	3.1	12.0	2.6
1-4 Mode	-	-	11.4	8.2
3-2 Mode	-	-	7.3	4.5
Overall attenuation	11.1	3.3	8.4	5.3

In configuration two, the overall attenuation level increased by 5.2 dB in the simulated results and by 2.7 dB in the experimental results. This increase was chiefly due to the additional control attained at 1-4 and 3-2 modes, which had only minimal control with one control force. Adding a second control force does actually increase the number of frequencies which are amplified in configuration two, especially between the 2-2 and 1-4 modes, but these frequencies are still 15 dB below the highest sound power levels on the plots. Thus they do not cause a significant overall amplification.

Similar results were seen in the additional configurations tested, but not shown in this paper. In these configurations, adding a second control force amplified some of the frequencies between modes, but attenuated the peaks better than a single controller. This shows that adding a second control force to the WSSG method of controlling a radiating simply supported plate makes the method more effective, and should be done where possible. The authors felt that adding a second control force can be implemented on most structures without significantly increasing the set-up time or complexity of the process.

Additionally, it was noted that the best control results were generally attained when the control shakers were located near the edges, and the WSSG sensor located near the center of the plate. Placing the shakers near the edges minimizes the mass loading and stiffness effects of the shakers, which causes fewer distortions in the WSSG field. Distortions will still occur though (especially near degenerate modes) and so it is desirable to place the WSSG sensor near the center. The center usually had a higher probability of being near unaltered antinodes for the WSSG terms, which gave better sound attenuation of the plate.

3.4 **Simply Supported Conclusions**

The results shown in this paper demonstrate that WSSG can be used to attenuate noise from a vibrating simply supported plate. Attenuation is achieved by minimizing WSSG at a single point on the plate through optimizing the amplitude and phase of a single control force. This attenuation can be increased by adding a second control force and keeping just the one WSSG sensor. The addition of the second control force helps attenuate noise coming from degenerate modes.

There were a few differences between the WSSG theory and the experimental data; two of which were the non-uniformity of WSSG at higher modes and smaller levels of attenuation

achieved than predicted. The theory of WSSG predicted that WSSG would be uniform across the face of the plate for individual modes. This did not completely hold for higher modes. Higher modes often did not have uniform values due to the superposition of degenerate modes and mass-loading effects.

The overall attenuation measured in the experimental results was less than the models predicted in every case. This was likely due to noise in the measurement of WSSG. The noise levels were such that in the simulations, a 10% to 20% difference was observed between the predicted noisy finite difference WSSG values and the analytical values. This limited the ability of the control algorithm to minimize WSSG and thus the ability to attenuate the noise emissions.

Despite these differences, significant control was still achieved. When two shakers were used, there was an overall attenuation of 3.28 dB for the first configuration and 5.34 dB for the second configuration. This represents a significant decrease in overall sound power levels. Thus WSSG should be considered as a viable alternative for use as a minimization quantity in active structural acoustic control of a simply supported plate. Although it may not be perfect, the ease of implementation and relatively unobtrusive nature of the sensors and actuators makes it more practical to use than most other minimization quantities.

4 EXPERIMENTAL RESULTS FOR A CLAMPED PLATE

This chapter outlines the experimental work which has been done on the use of WSSG as the minimization quantity in control of a vibrating clamped plate. The setup of the experiment is shown, followed by images of WSSG measured across the surface of the plate for several modes. This was done to validate the theoretical development for WSSG as a uniform field over the plate. Control plots are shown for the experimental setup and the results are discussed. It is important to note that the theoretical development for WSSG on a clamped plate was not performed by Fisher *et al.*[15] This was instead done by Johnson[19] and a brief synopsis of this research is presented in Section 4.1.

4.1 Brief Synopsys of the WSSG Theory for Clamped Plates

The derivation for WSSG on clamped plates followed the same process as simply supported plates. The major difference is that there are no exact analytical equations which model a vibrating clamped plate. An approximate analytical solution was instead implemented using a method assuming the product of beam mode shapes as the approximate eigenfunctions of the plate[20, 21]. This allowed the same derivatives ($\frac{\partial w}{\partial x}$, $\frac{\partial w}{\partial y}$ and $\frac{\partial^2 w}{\partial x \partial y}$) to be calculated and used to derive the individual terms of WSSG. The general equation for WSSG stays the same as Eq. 1-2 but the weights were modified. The clamped weights were calculated in the same method as the

simply supported weights and Table 4-1 shows the clamped WSSG weights. An average over the modes of interest was also used when multiple frequencies were being controlled.

Table 4-1: Clamped Scaling Factors

α	$\beta[m^2]$	$\gamma[m^2]$	$\delta[m^4]$
1	$\left(\frac{L_x}{\lambda_m}\right)^2$	$\left(\frac{L_y}{\lambda_n}\right)^2$	$\left(\frac{L_x L_y}{\lambda_m \lambda_n}\right)^2$

The subscripts m and n represent the structural mode numbers and the values for λ_i are given by the characteristic equation,

$$\cosh(\lambda_i)\cos(\lambda_i) = 1. \tag{4-1}$$

A more generic method of calculating the weights regardless of boundary conditions was determined and is shown in Table 4-2, where k_x and k_y represent the wave numbers in the x and y directions, respectively.

Table 4-2: Generic Scaling Factors

α	$\beta[m^2]$	$\gamma[m^2]$	$\delta[m^4]$
1	$\left(\frac{1}{k_x}\right)^2$	$\left(\frac{1}{k_y}\right)^2$	$\left(\frac{1}{k_x k_y}\right)^2$

It was hoped that when the correct weights were applied to the four individual WSSG terms and the total WSSG field calculated, that a nearly uniform quantity would be seen, similar to simply supported plates. However, the resulting WSSG field was shown to be more uniform than merely taking the transverse velocity field, but it was not as uniform as the simply supported plates. This is due to the clamped boundary conditions around the edge which limits both the transverse movement and rotation (and therefore the spatial derivatives). This means

WSSG approaches zero near the edges of the plate. This limits the uniformity of WSSG on a clamped plate.

4.2 **Experimental Setup**

A plate was assembled using 6061-T6 rolled aluminum; a list of the properties is given in Table 4-3. The clamped boundary condition was created by placing the plate between two stiff frames and bolting the frames together. A picture of the plate is shown in Fig. 4-1. Spatially dense velocity measurements across the entire plate were made with an SLDV to ensure the clamped boundary conditions were met.

The plate was excited with a Labworks ET-126 shaker attached to a signal generator and controlled with a Bruel and Kjaer type 4809 Vibration Exciter. These shakers were suspended from a stiff frame and attached to the plate by gluing the individual stingers to the back side of the plate. WSSG was measured at a point using four accelerometers placed 0.0254 m apart in the configuration shown in Fig. 2-2. The accelerometer signals were put through a filter and into a DSP controller which calculated WSSG using Eqs. 1- 2, and 2-1 through 2-4.

Table 4-3: Properties of the Clamped-Clamped Plate .

Property	Value
Length (x direction)(L_x)	0.483 m
Length (y direction)(L_y)	0.762 m
Thickness (h)	0.0031 m
Young's modulus (E)	68.9 GPa
Poisson's ratio (ν)	0.334
Density (ρ)	2700 Kg/m^3
Damping ratio (η)	2%

Figure 4-1: The Clamped-Clamped Plate

Control was achieved using a modified Filtered X LMS algorithm in the DSP controller which optimized the phase and amplitude of the control shaker to minimize WSSG. The SLDV was used to measure the velocity at an array of points on the plate and then sound power was calculated using the method of elementary radiators[2]. A full schematic of the experimental set up is shown in Fig. 3-2. The plate was then placed in a window between two large acoustic reverberation chambers. This provided a baffle between the two sides of the plate and isolated the plate from any outside vibrations or noises.

4.3 Experimental Validation of the WSSG Theory

The theoretical development of WSSG as a uniform parameter was validated by scanning the vibrating clamped plate with the SLDV at the natural frequencies. This was done without the normal disturbance or control shakers attached; a small LDS V203 shaker was used

instead. The individual terms of WSSG were calculated for each of the modes. The four WSSG terms for the first mode are shown in Fig. 4-2.

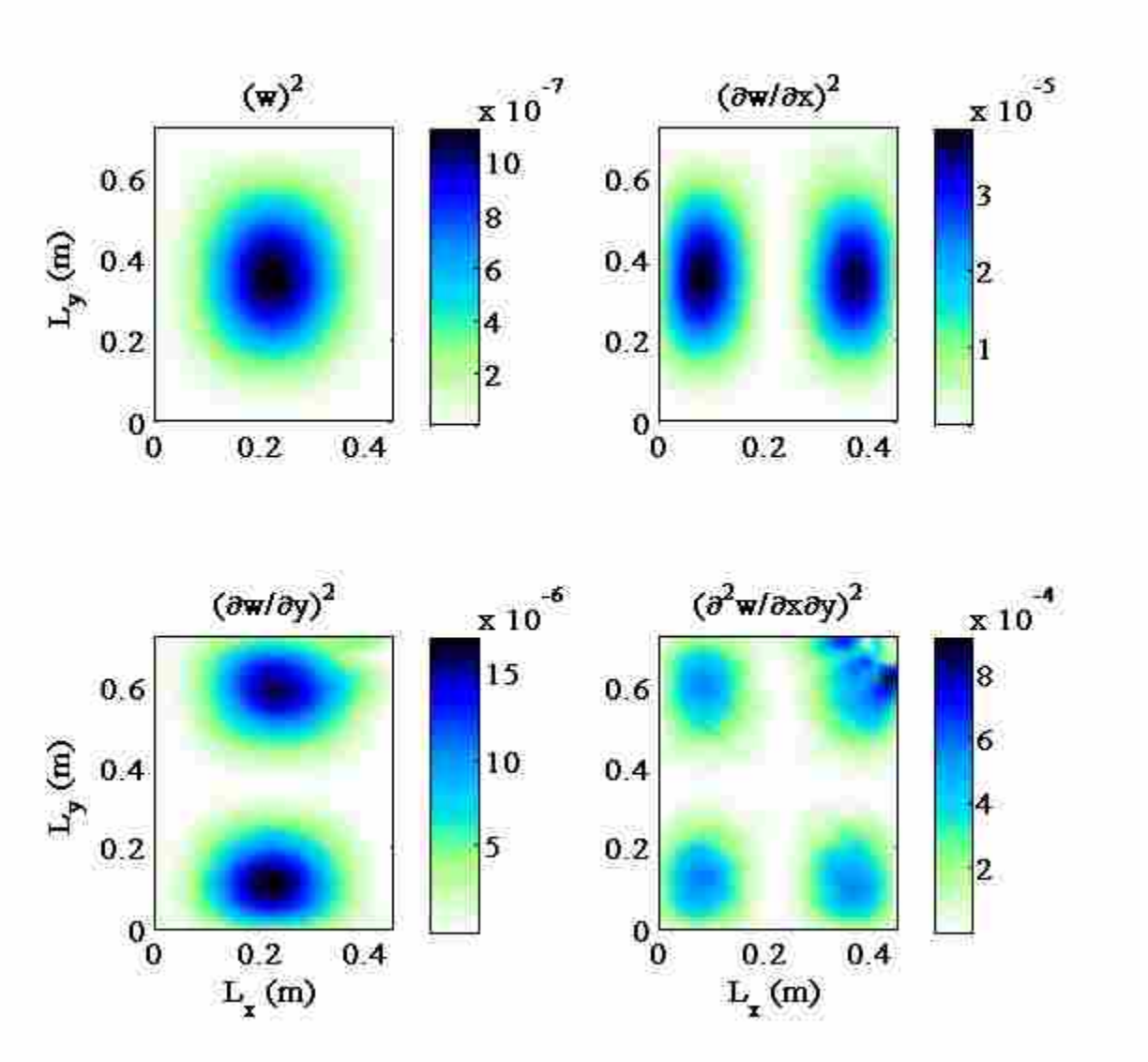

Figure 4-2: Plots of the Four WSSG Terms of the First Mode

The four terms shown here closely match the four shown by Johnson[19]. These terms are similar to the ones shown for the simply supported plate, except that all four terms are driven to zero at the boundary. On simply supported plates the last three terms all carried values through to the edge of the plate.. Figure 4-3 shows the combined WSSG field for the 1-1 mode of the clamped plate.

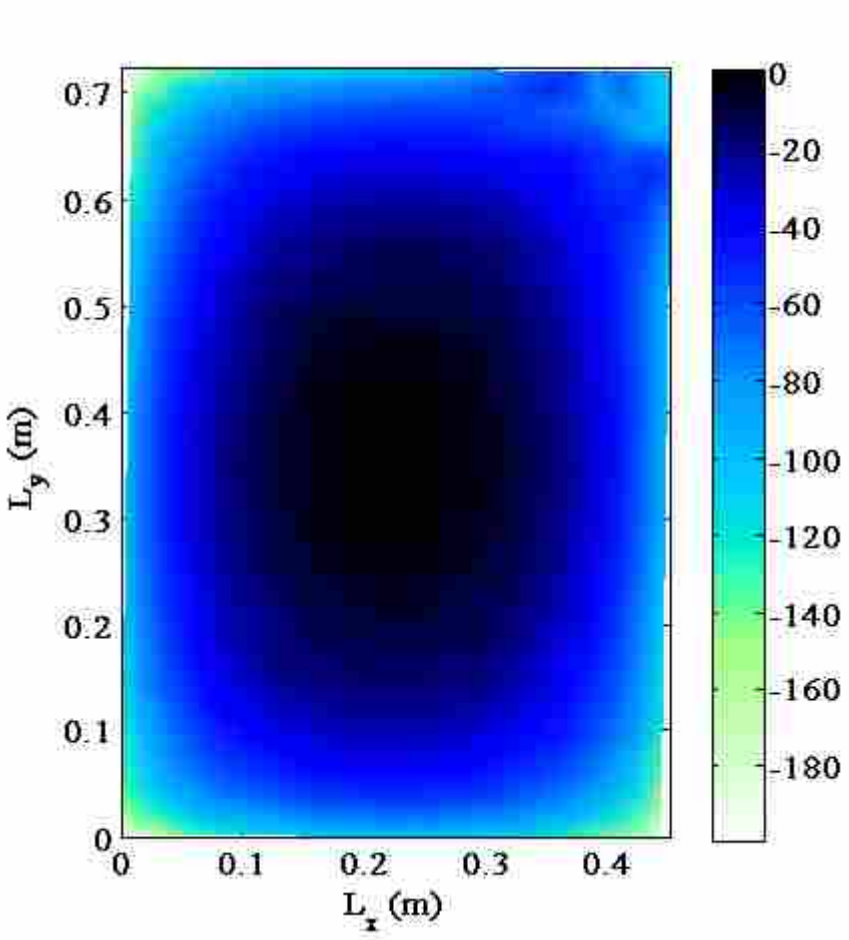

Figure 4-3: Total WSSG Field from the 1-1 Mode in dB (re max value on the plate), with Frequency Specific Weights

Figure 4-3 shows that WSSG on a clamped plate is more uniform than simply measuring the transverse velocities, but it is not as uniform for the clamped plate as it was for the simply supported case. Figure 4-4 shows plots of the combined WSSG fields for the next four modes when the ideal mode-specific weights are used. These modes show that the WSSG field generally becomes more uniform when higher modes are present on the plate. This is because the zone affected by the clamped edge conditions on the plate gets smaller as higher modes are present. This allows WSSG to be more uniform across more of the plate.

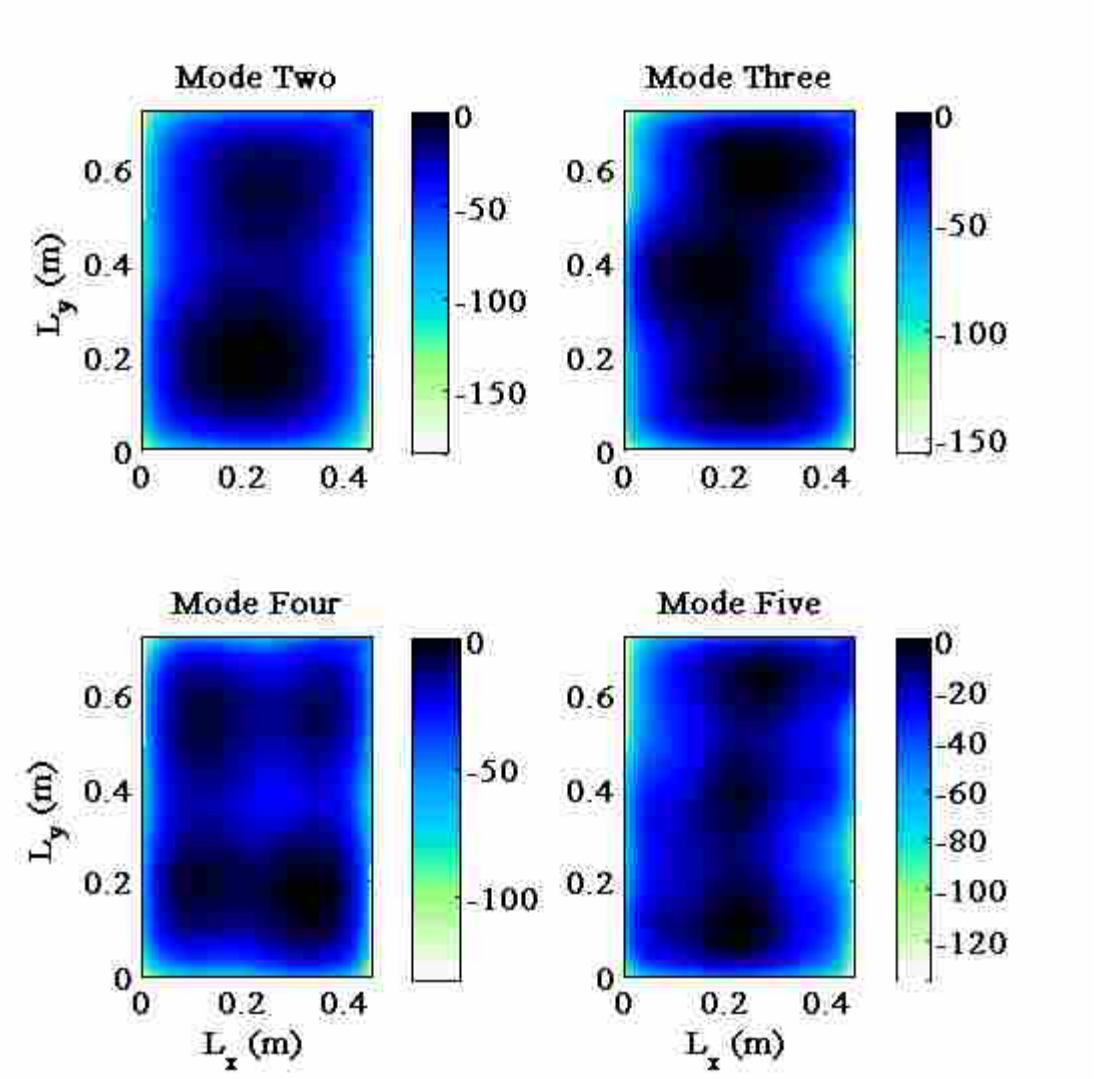

Figure 4-4: Plots of WSSG for Modes Two-Five in dB (re max value on the plate)

The experimental results did have more non-uniformities in the WSSG field than the theory predicted. The non-uniformities on each of these plots can be traced to the non-uniform amplitudes of the anti-nodes. The computer simulation predicted that each anti-node would have uniform amplitudes, but this is not always the case in experimental data. For example, on the second mode (the 1-2 mode), the shaker is located in the lower right corner of the plate, much closer to the lower anti-node than the upper. The SLDV scans showed that this caused the lower anti-node to have a slightly higher amplitude than the upper anti-node, which makes it

impossible for the same WSSG values to be calculated. However, the amplitudes are close enough in value (for the 1-2 mode) that placing the WSSG sensor in either quadrant will still cause significant sound attenuation of the mode. This is not the case for some of the other modes, where higher amplitude differences were measured between the anti-nodes.

Some of the higher modes had larger variations in the anti-node amplitudes because of overlap between resonant frequencies. When two resonant frequencies are closely spaced their mode shapes often superimpose on top of each other, causing distortions in the mode shapes. These can cause significant differences in the anti-node amplitudes, which causes WSSG to lose some of its uniformity. Thus, whenever a resonant frequency was isolated (far away from any other natural frequency) a more uniform WSSG field was calculated, but when natural frequencies were close to each other, the WSSG field was less uniform. Some of these non-uniform effects had been predicted by the computer simulations but the experimental results showed even more pronounced amplitude differences.

4.4 **Experimentally Measured Sound Power Results**

The plate was set up in the configuration shown in Fig. 3-2 with the disturbance shaker (F_d), control shaker (F_c) and sensor (S) located at $F_d = (0.083, 0.629)$ m, $F_c = (0.083, 0.127)$ m, and $S = (0.340, 0.162)$ m. Sound power measurements were taken on the experimental plate before and after WSSG control. A computer simulation was built using the clamped plate approximations mentioned at the beginning of the chapter and control simulations were run in order to compare the WSSG theoretical results to actual experimental results. These simulated control plots are shown in Fig. 4-5. The experimental results are shown in Fig. 4-6.

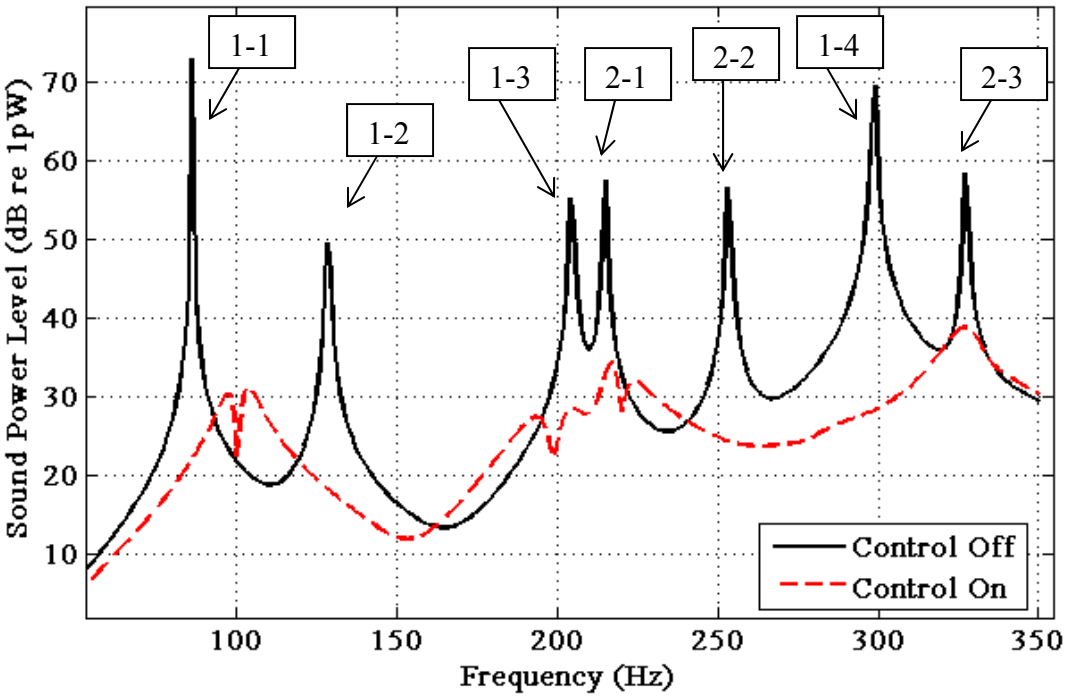

Figure 4-5: Simulated Control of the Clamped Plate with One Control Shaker

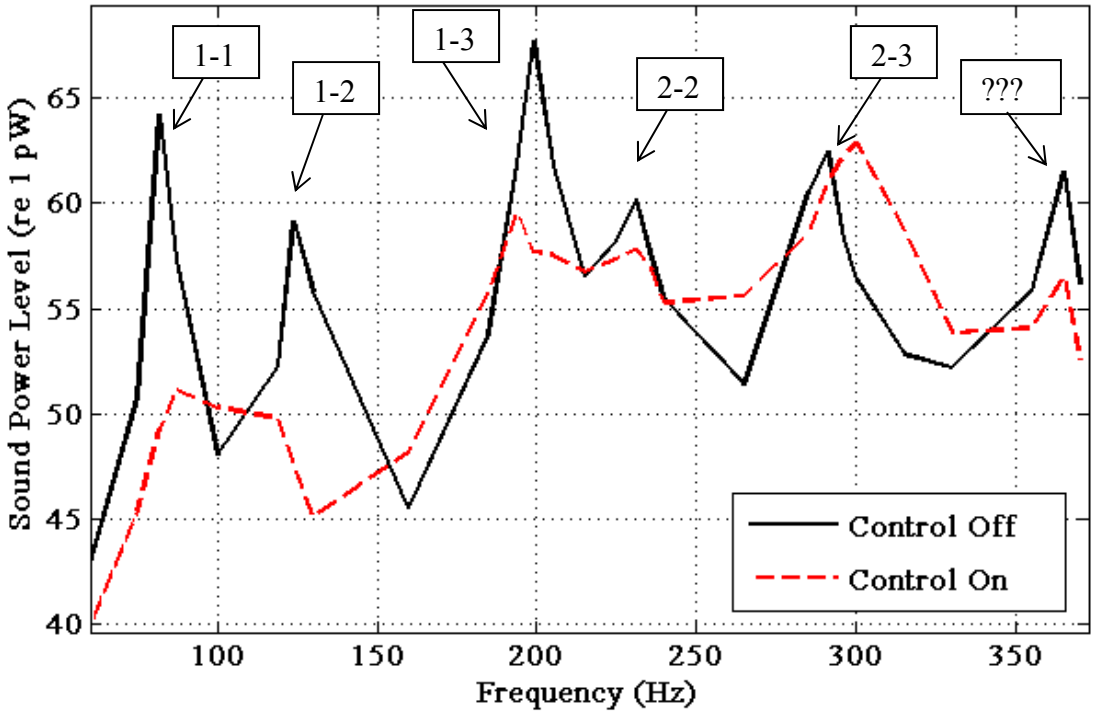

Figure 4-6: Experimental Control of the Clamped Plate with One Control Shaker

The simulated results were made with a frequency increment of 1 Hz, while the experimental tests were made with a varying frequency increment. The frequencies were chosen by performing a broadband SLDV scan of the vibrating plate when it was being excited with white noise. The broadband SLDV scans were made with a frequency resolution of 1.25 Hz. This allowed the author to identify each of the resonant peaks and then run WSSG based control tests at the resonance peaks and several of the nearby frequencies (+- 5 Hz). For example, if a resonance was discovered at 200 Hz, then WSSG based control tests were run at 195, 200, and 205 Hz. Additional tests were performed in between the resonance peaks in order to capture the general shape of the sound power plots.

Table 4-4 shows the attenuation levels achieved at each resonance frequency for both the analytical and experimental plots, as well as the overall attenuation levels.

Table 4-4: Attenuation Levels for Configuration One, Clamped Plate

	Attenuation Levels (dB)	
Mode	Simulation	Experimental
1-1 Mode	51.2	13.1
1-2 Mode	31.3	11.7
1-3 Mode	26.6	10.2
2-1 Mode	23.2	-
2-2 Mode	32.3	2.4
1-4 Mode	41.3	-
2-3 Mode	19.7	1.4
??? Possibly 2-4 Mode	-	5.0
Overall attenuation	25.0	4.3

Several differences between Figs 4-5 and 4-6 are apparent and they present challenges to comparing the two tests. The first difference is that several of the experimental resonance

frequencies are shifted from the simulated results. There appears to be a general downward shift in frequencies which would be consistent with the idea that the shifts are caused by mass loading from the shakers. An example of this can be seen by looking at the 2-2 mode, which appears at 253 Hz in the simulation but is shifted down to 231 Hz in the experimental plots.

A second key difference between Fig. 4-5 and 4-6 is that the experimental results appear to be missing several of the resonant frequencies which exist in the simulations. There are two probable reasons for these resonances to be missing: the experimental sampling resolution may not have been high enough to differentiate between two closely spaced resonant frequencies, or the added mass and stiffness from the shakers may have distorted the structural modes in such a way that they were no longer a recognizable mode shape. It is possible that both reasons could be playing a role in causing the missing resonances.

For example, in Fig. 4-6 the resonance peak shown at 200 Hz was shown in the SLDV scans to be an easily recognizable 1-3 mode shape. However, the 1-3 mode shape was not perfect and it appeared that a very weak 2-1 mode shape might have been located nearby, causing slight distortions to the 1-3 mode. The 2-1 mode may have had a small enough amplitude that it did not show up as a significant independent structural mode in the broadband SLDV scans, but it was still able to cause minor distortions to the surrounding frequencies. A similar thing may have happened with the mode at 291 Hz in Fig. 4-6, which was a clearly recognizable 2-3 mode (see Fig. 4-7) but which may have been distorted by a nearby 1-4 mode. A clearly recognizable 1-4 mode was not seen in the SLDV scans at any point, but it may have still been present on the plate at a small amplitude.

The mode shape at 365 Hz (Fig. 4-6) was unrecognizable, although it may have been a highly distorted 2-4 mode. The analytical model predicted that a 2-4 mode should appear after the 2-3 mode, but the 2-4 mode shape was indistinguishable in the SLDV scan.

Despite these differences, several important concepts about the use of WSSG in experimental setups for clamped plates. The first is that Fig. 4-5 and 4-6 have the same general trends and shapes when the "Control On" lines are compared: both have significant attenuation at most peaks, and both have minimal amplification at some frequencies between peaks. The experimental attenuation levels were significantly lower than the analytical levels in much the same way as was seen in the simply supported plots. This is possibly due to noise in the signals which limits the ability of the DSP to find the "optimal" amplitude and phase of the control signal. The distortions to the WSSG field from overlapping structural modes also likely limited the effectiveness of WSSG in the experimental setup in a manner which was not predicted in the simulations.

One resonance frequency of particular interest was the 2-3 mode, where the experimental results show a minimal attenuation at the peak itself and then amplification directly following the peak. This contrasts with the simulated results which predicted 19.7 dB of attenuation and no amplification afterward. The mode was analyzed in an attempt to explain the poor experimental results. It was determined that the experimental 2-3 mode was significantly distorted, causing several of the anti-nodes to have significantly lower amplitudes. Two of the six anti-nodes had much lower amplitudes than the other four (See Fig. 4-7, No Control). When the mode was being controlled, the four high anti-nodes were minimized but the areas with low amplitudes were suddenly amplified. This is shown in Fig. 4-7, which shows the squared velocities of the plate at the 2-3 mode before and after control.

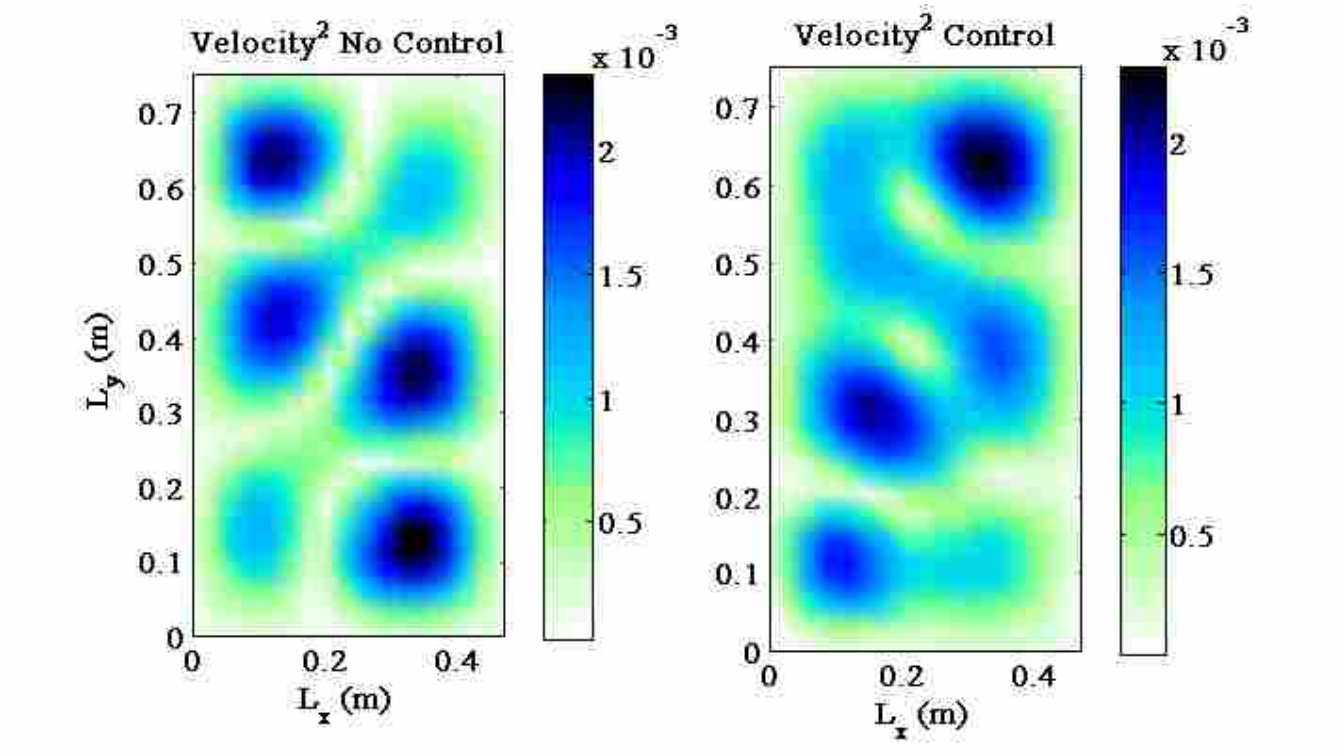

Figure 4-7: Experimental Velocity Field for the 2-3 Mode, with Control Off and Control On

Thus, minimizing WSSG brought down the amplitudes of all the high anti-nodes but amplified the amplitudes of the lower anti-nodes. These velocity amplitude differences are reflected in the plots of WSSG and explain why little attenuation was achieved. Figure 4-8 shows the plots of WSSG before and after control for the 2-3 mode.

WSSG theory assumes that the WSSG field is uniform across the entire plate. Thus minimizing one point will, in theory, minimize WSSG across the entire plate. But if the WSSG field is not uniform across the plate, then minimizing a single point may end up amplifying the areas which were originally lower. This means little control may be achieved overall because the plate will simply begin to radiate from a different place on the plate. This effect was also seen for the frequencies directly following the 2-3 mode, where overall amplification was observed.

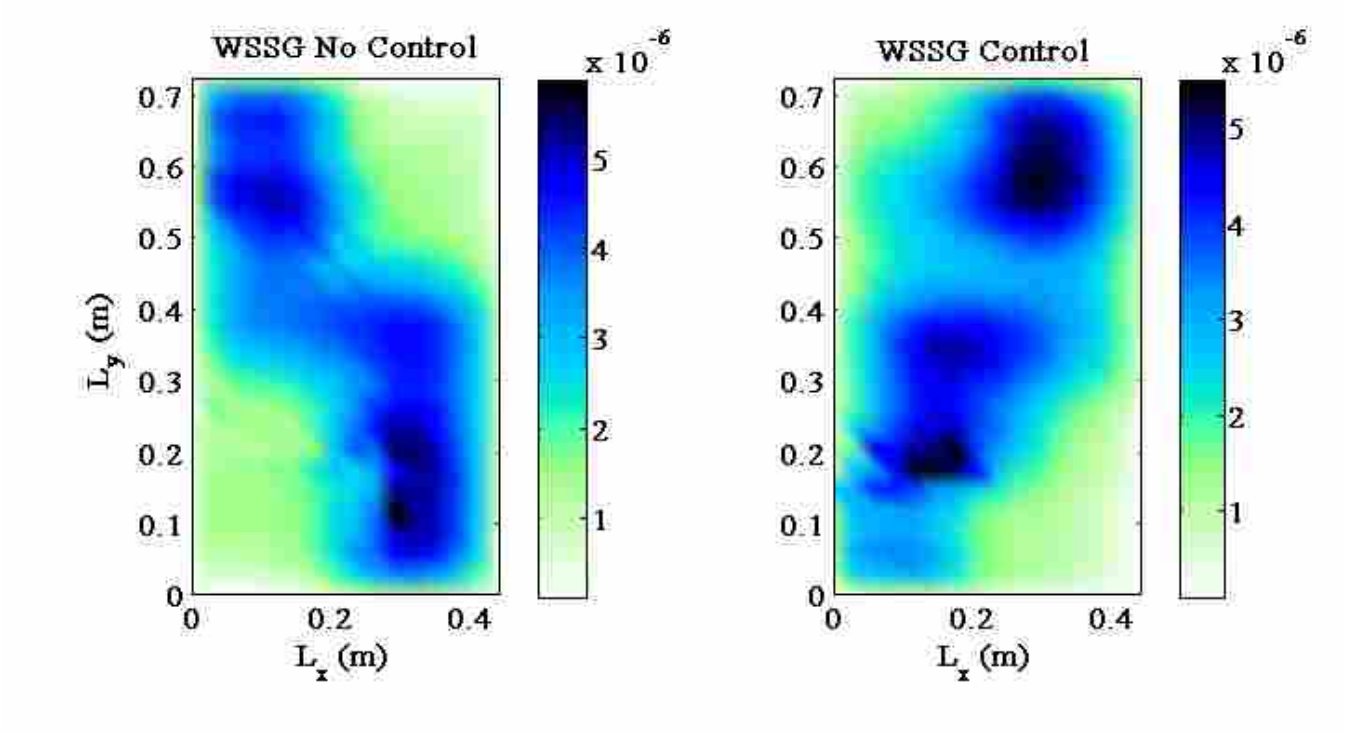

Figure 4-8: Experimental WSSG Field for the 2-3 Mode, with Control Off and On

The distortion of the 2-3 mode was visible in the scans performed in section 4.3 when only a single lightweight shaker was attached the plate (see Fig. 4-9), which implies that mass loading is not the primary source of the distortion. However, when the two heavy shakers at attached to the plate the uniformity of WSSG appears to become worse, suggesting that mass loading effects are still contributing minimally to the distortion. This is shown by comparing Fig. 4-8 "WSSG No Control" to Fig. 4-9. A perfect comparison cannot be made between these two figures because they had different forcing amplitudes, but the single lightweight shaker plot appears to be more uniform than the two heavy shakers plot (especially in the top right and lower left corners). These two figures were also plotted by the author on a dB scale (re the highest WSSG value on each respective plate). These plots are not shown here but on the dB plots the lightweight WSSG plot had approximately 95% of the entire plate within 3 dB of the maximum, while the two heavy shaker WSSG plot had approximately 65% of the entire plate within 3 dB of

the maximum. This means the addition of the two heavy shakers did negatively affect the uniformity of the WSSG field.

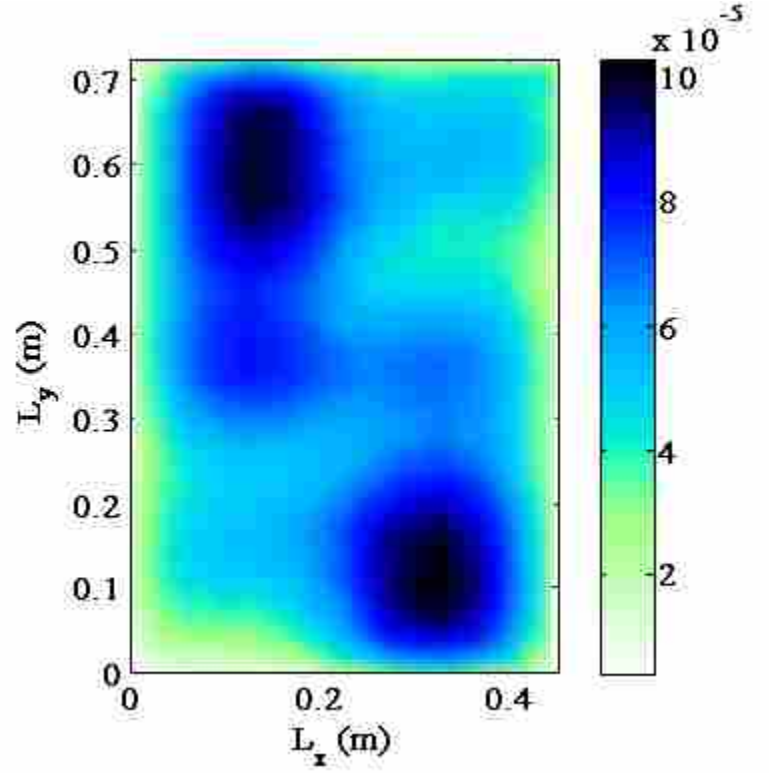

Figure 4-9: Experimental WSSG Field for the 2-3 Mode with a Single Lightweight Shaker

The author theorizes that these effects could be minimized if the mass and stiffness effects of the shakers could be negated somehow. This could possibly be done by using smaller shakers. Doing this would help the WSSG field remain more uniform and it's possible that fewer areas would be amplified when WSSG was minimized at a point.

It was noted in Chapter 2 that adding a second control force improves the overall attenuation on a simply supported plate and so a decision was made to try it on the clamped plate as well. However, the decision to add a second control shaker was not made until after the original setup had been taken down. Thus a new single shaker control plot had to be created and then a second control shaker added to the new setup. These plots were made with the disturbance

shaker (F_d), control shaker one (F_{c1}), control shaker two (F_{c2}) and sensor (S) located at $F_d = (0.39, 0.64)$ m, $F_{c1} = (0.13, 0.63)$ m, $F_{c2} = (0.41, 0.13)$ m and $S = (0.19, 0.28)$ m.

The results of the new configuration are shown in Figs. 4-10 and 4-11. Table 4-5 shows the overall attenuation levels for both one and two control shakers, as well as the attenuation levels for each individual resonance frequency.

Table 4-5: Attenuation Levels for Configuration Two, Clamped Plate

	Attenuation Levels (dB)	
Mode	One Controller	Two Controllers
1-1 Mode	35.28	10.66
1-2 Mode	24.71	14.98
1-3 Mode	10.98	8.13
2-2 Mode	1.01	1.55
2-3 Mode	-4.07	4.27
Unknown Mode	-0.07	2.85
Overall attenuation	2.89	4.29

The placement of the shakers in configuration two caused the resonance frequencies to shift upward from configuration one. Table 4-6 shows the observed resonant frequencies for configuration one and configuration two. All resonant frequencies were shifted for the second configuration which implies that the shaker locations can affect the plate resonances.

Table 4-6: Resonant Frequencies for Configuration One and Configuration Two

Mode	1-1	1-2	1-3	2-2	2-3	Unknown
Frequency (Hz) Config. 1	81	122	188	223	286	390
Frequency (Hz) Confg. 2	82	124	199	231	291	365

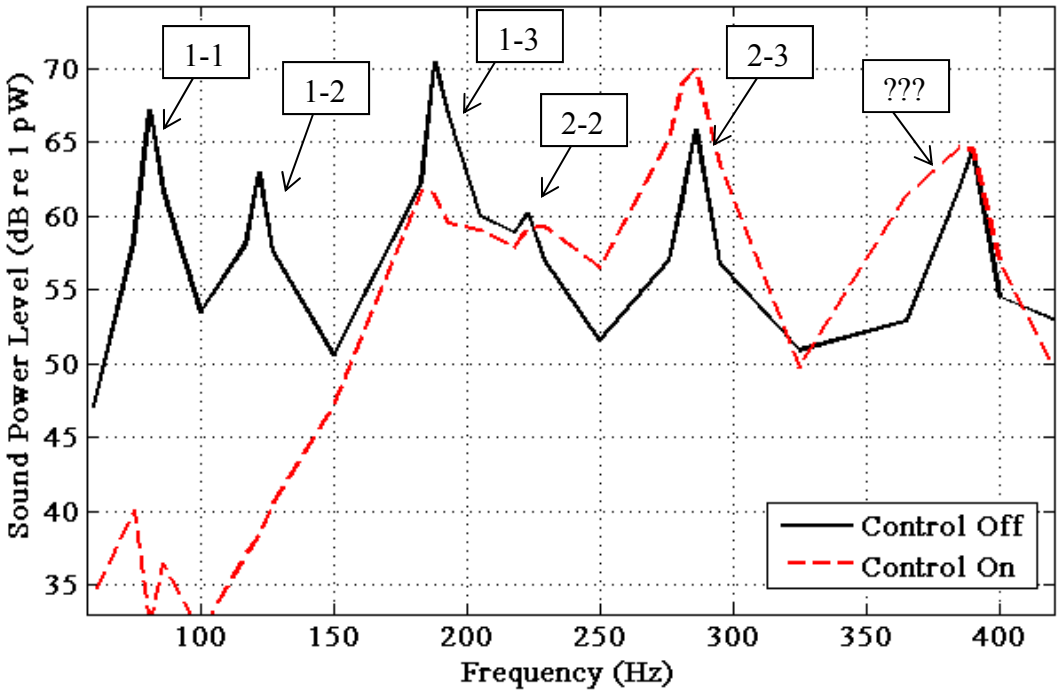

Figure 4-10: Experimental Control of a Clamped Plate in Configuration Two with One Control Force

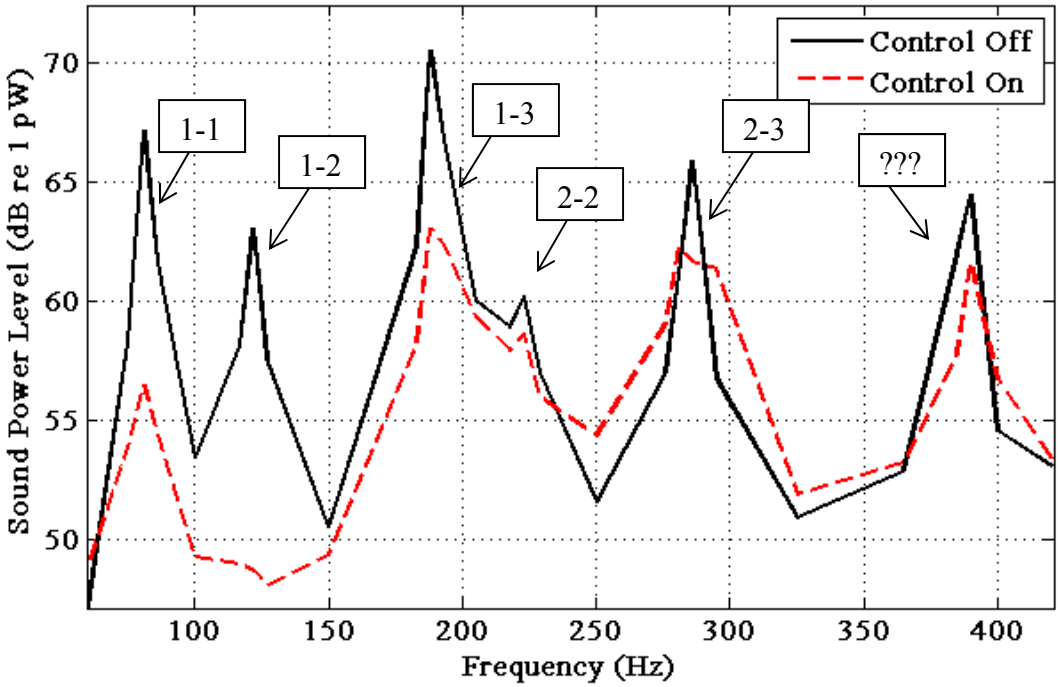

Figure 4-11: Experimental Control of a Clamped Plate in Configuration Two with Two Control Forces

In both these plots, the 1-3 mode was not perfect, and may actually be a combination of the 1-3 and the 2-1 mode. The 2-3 mode was severely distorted near the top of the plate and may also have been influenced by another mode. The unknown mode was not entirely clear in either configuration, but it may have been a distorted 2-4 mode.

Figure 4-11 shows that adding a second control shaker gives better control results, but it does not make the results perfect. In the one-control shaker plot (Fig. 4-10) there was control of the first four visible peaks, but none for the fifth (2-3 mode) and sixth (unknown mode). The 2-3 mode was actually amplified with one control shaker. In the two-control shaker plots, some control was lost at the lower peaks but the last two modes were both attenuated by at least 3 dB. Overall, the total sound power attenuation levels increased from 2.9 dB (one controller) to 4.3 dB (two controllers). This increase is primarily due to the increased control achieved at the 2-3 mode. Thus, it is shown that adding a second control shaker can be used to improve the overall attenuation for a vibrating clamped plate.

4.5 **Clamped Plate Conclusions**

The experimental results shown in this chapter show that the WSSG theory developed by Johnson[19] can be used to control a vibrating plate. The total WSSG field is not as uniform as it was for a simply supported plate but it is still uniform enough to achieve control results. The experimental results shown in this paper were not as good as computer simulations but this is likely due to random noise in the signals and the fact that the computer simulations did not predict much distortion to the structural modes. Several of the experimental modes were highly distorted, which decreased the uniformity of WSSG and its ability to attenuate noise. The WSSG-based control method appears to be an effective manner for attenuating sound power radiated from a clamped plate if the plate has clean (non-distorted) structural modes.

5 EXPERIMENTAL RESULTS FOR A RIBBED PLATE

This section details the experimental results for WSSG-based control of a ribbed plate with simply supported boundary conditions and free ends on the ribs. There were two ribs on the plate, located at $x = L_x/3$ and $x = 2L_x/3$. The theory for WSSG on a ribbed plate was also studied by Johnson[19]. The first section of this chapter is a brief synopsis of some of the important theoretical changes made to the WSSG theory so that it can be applied to a ribbed plate.

5.1 Brief Synopsis of the WSSG Theory for Ribbed Plates

There are no analytical equations or approximations which can be used to calculate the displacement of a vibrating ribbed plate and so the theory behind WSSG for ribbed plates had to be modified some. Instead of calculating the weights by taking the derivatives, a new method had to be found. It was determined that the purpose of the weights in the simply supported and clamped plates was to make the amplitudes of each of the four WSSG terms contribute equally to the total summed WSSG. Thus scaling factors could theoretically be determined by simply optimizing them until this was achieved. The easiest way to do this was to measure the vibrations of a ribbed plate using FEA or the SLDV and then use the finite difference equations to back out the four un-weighted WSSG terms. The maximum values of each term were then measured and the terms were scaled such that they all had the same maximum value. This caused the total WSSG field to be nearly uniform.

Computer simulations were developed using finite element analysis to study the effectiveness of WSSG as a minimization quantity in ASAC on a ribbed plate. These results showed that WSSG-based control of ribbed plates was comparable to volume velocity-based control of ribbed plates. Similar levels of attenuation were discovered for both methods, but WSSG was able to achieve the results using few sensors.

Johnson[19] gave several recommendations for using the WSSG-based control method on ribbed plates. It was recommended that the control shaker be placed within the same "bin" as the disturbance shaker (a "bin" is one of the three areas on the plate separated from the rest of the plate by a rib). Placing them in different bins often amplified the radiated sound power at some of the resonant frequencies. The placement of the sensor was shown to be more robust and attenuation was achieved if the sensor was placed in any of the three "bins." However, more attenuation was achieved if the sensor was located in the same bin as the two shakers.

5.2 **Experimental Setup**

The basic set up for the experimental ribbed plate is the same as for the simply supported and clamped plates. The ribbed plate was created from 6061-T6 rolled aluminum with the same properties as the simply supported plate. The only difference was the two ribs glued to the plate using an epoxy resin. The ribs were made from the same material and are the same thickness as the original plate. A picture of the plate is shown in Fig. 5-1.

Figure 5-1: The Ribbed Plate

The plate was set up in the configuration shown in Fig. 3-2 with the disturbance shaker (F_d), control shaker (F_c) and sensor (S) located at $F_d = (0.438, 0.692)$ m, $F_c = (0.422, 0.067)$ m and $S = (0.375, 0.464)$ m.

5.3 Experimental Validation of the WSSG Theory

The four terms of WSSG were measured for multiple natural frequencies using the SLDV and then plotted to verify the uniform nature of the total WSSG quantity. It was discovered that the four terms of the first mode closely resembled the simply supported results, and a nearly uniform total WSSG field was observed. The four WSSG terms of the first mode are shown in Fig. 5-2 and the summed WSSG field in Fig. 5-3.

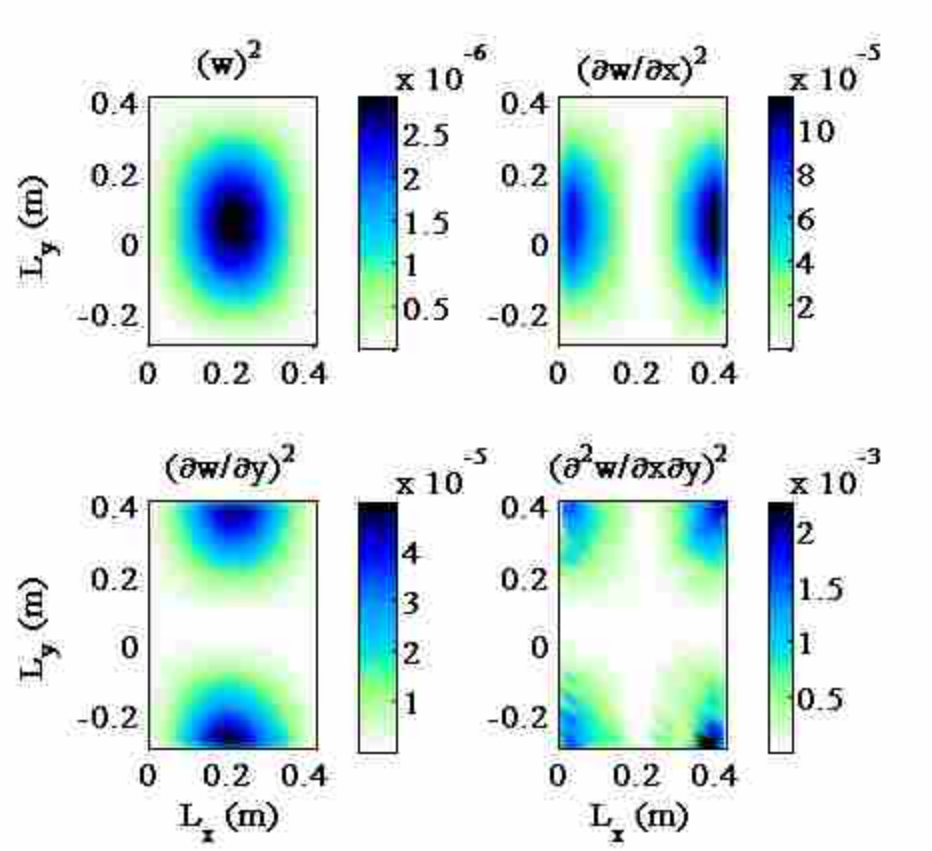

Figure 5-2: The Four WSSG Terms for the 1-1 Mode of a Ribbed Plate

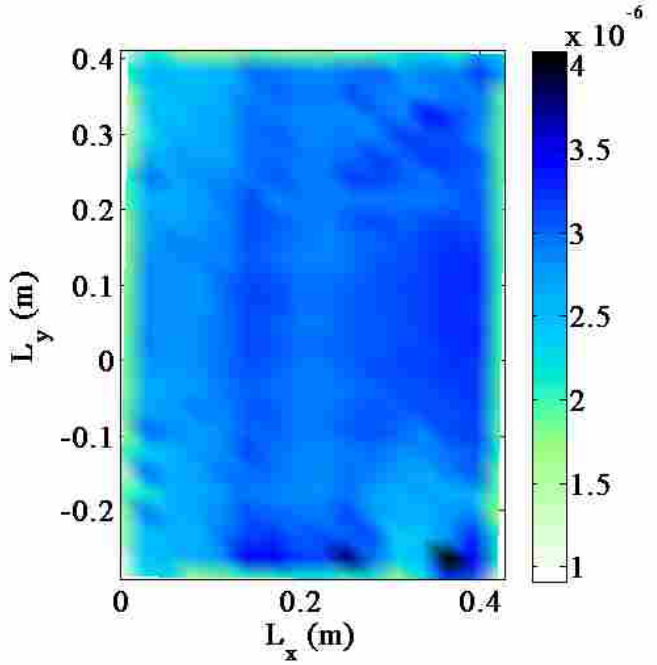

Figure 5-3: Total WSSG Field for the 1-1 Mode of a Ribbed Plate

The ribs on the plate did not significantly distort the 1-1 mode. Its shape very closely resembled that of the 1-1 mode of the simply supported plate. This was also true for the 1-2 mode. WSSG was nearly uniform across the plate and there appeared to be little difference between the simply supported plate and the ribbed plate other than the amplitude of the structural vibrations.

Once the higher modes were reached the ribs began to alter the structural mode shapes and the WSSG field was distorted significantly. This is shown in the 2-2 mode. The four WSSG terms of the 2-2 mode are shown in Fig. 5-4 and the total summed WSSG shown in Fig. 5-5.

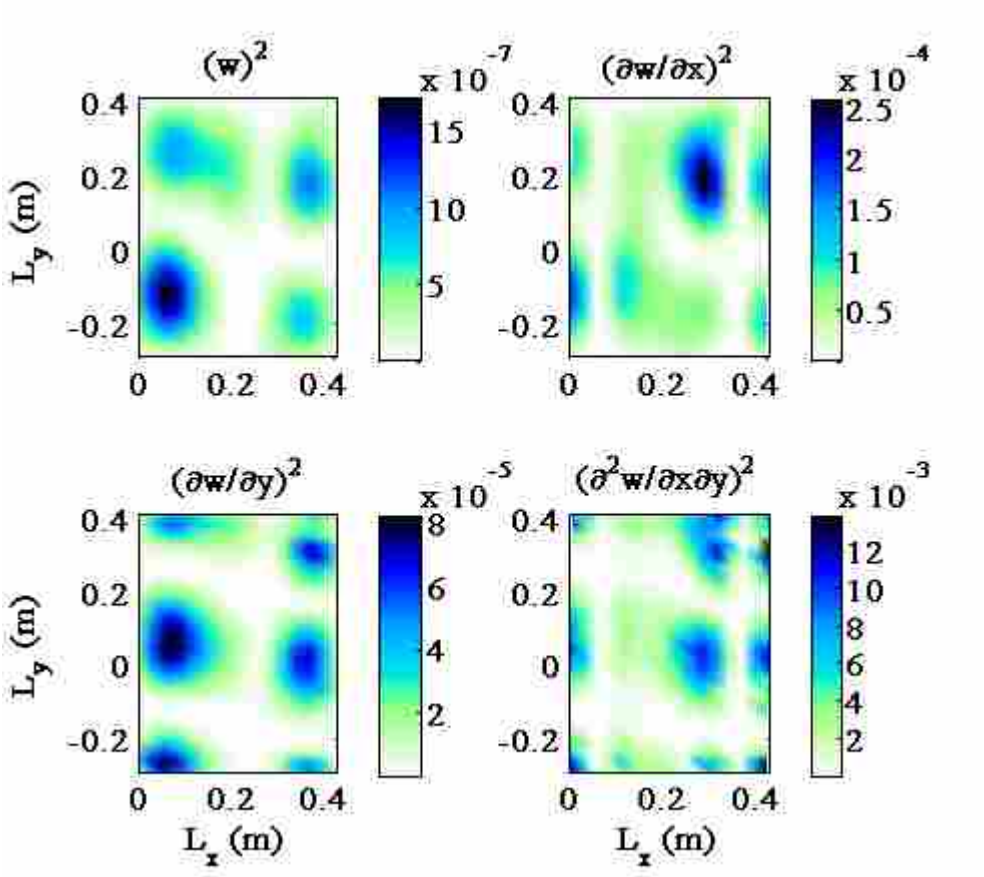

Figure 5-4: The Four WSSG Terms for the 2-2 Mode of the Ribbed Plate

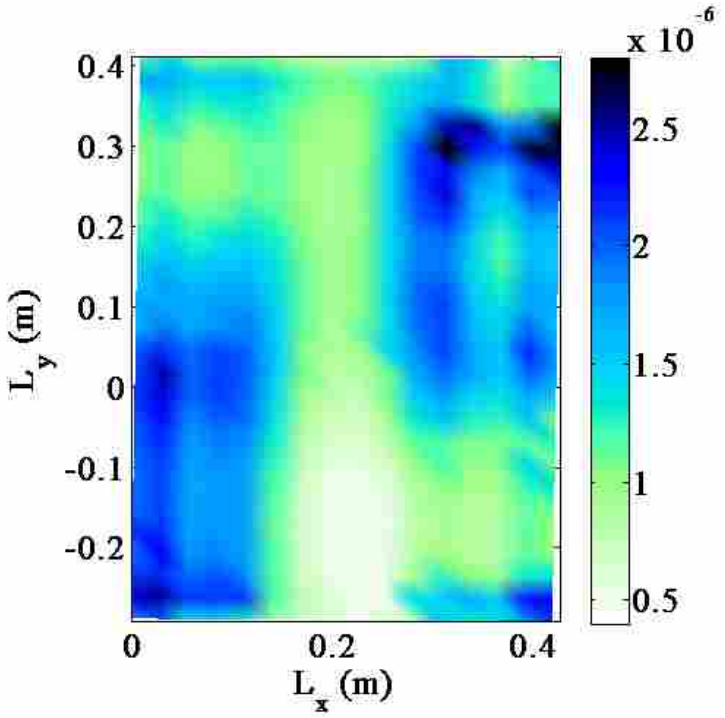

Figure 5-5: The Total WSSG Field for the 2-2 Mode of the Ribbed Plate

Figure 5-4 shows that the ribs distort the 2-2 mode such that the four anti-nodes are "squeezed" into the two side bins, leaving the center bin with very small amplitudes. This in turn affects the four individual WSSG terms, causing none of them to have significant contributions to the WSSG field in the center bin. Thus, a sensor placed in the center bin would not capture the true WSSG field. Some control can still be attained, but better results are obtained if the sensor is placed in one of the side bins. The configuration studied in this chapter has the sensor placed in the far right bin, along with both shakers.

Figure 5-6 shows the simulated control results for the ribbed plate. This control plot was created by Yin Cao using ANSYS. The experimental control results are shown in Fig. 5-7 and were measured by the author.

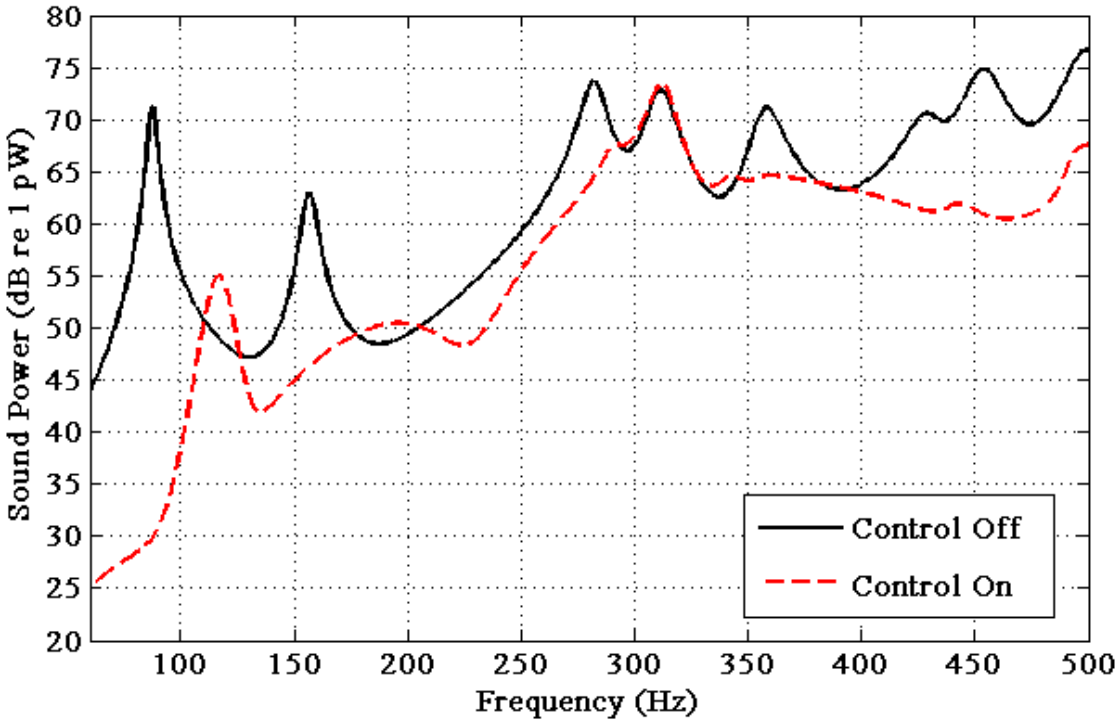

Figure 5-6: Finite Element Sound Power Results for Control of a Ribbed Plate with One Control Force

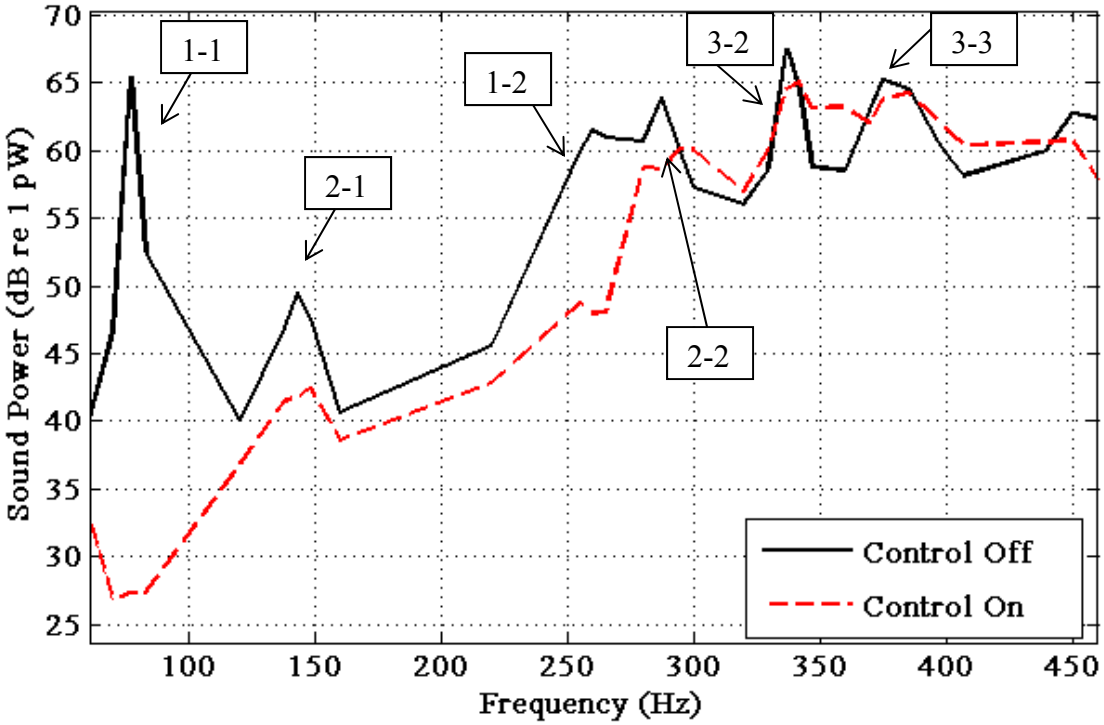

Figure 5-7: Experimental Sound Power Results For Control of a Ribbed Plate with One Control Force

The results shown in Figs. 5-6 and 5-7 are similar to the ones shown for both the simply supported and clamped plate conditions. Control was achieved in modes where the resonant frequencies were spaced far apart and in the places where the structural modes had uniform anti-nodes. Where degenerate modes or any form of non-uniformities in the structural anti-nodes existed, then the WSSG control results suffered. An overall experimental sound power attenuation level of 4.9 dB was calculated for this plate.

Single control force tests were run with the shakers and sensor in a variety of configurations to validate the recommendations given by Johnson[19]. It was confirmed that the best control results were attained when all three components were in the same bin. If the shakers were placed in adjoining bins then the control results usually amplified the sound power radiated on many of the peaks. This was especially true on the structural modes which had two anti-nodes in the x direction ($m = 2$). In these situations, the ribs on the plate distorted the anti-nodes in such a way that there would be little-to-no movement whatsoever in the center bin and the two anti-nodes would instead be confined to the outer two bins. Placing a control shaker in the center bin could not adequately excite the two structural modes in the x direction and instead caused the center bin to vibrate with higher amplitudes than had been excited before. This caused an amplification of the radiated sound power.

It was also determined that the placement of the four accelerometers to measure the spatial gradient could not be placed near one of the ribs. The ribs caused distortion to the WSSG field and so the sensor needed to be placed away from those distortions for a more accurate reading.

5.4 **Ribbed Plate Conclusions**

It is important to note that the information learned in these experimental tests relate to the control of a simply supported plate with two free ribs located at $x = L_x/3$ and $x = 2L_x/3$. The conclusions reached in this chapter may relate to other configurations of ribbed plates, but further tests would be required before definitive statements can be made.

It was shown in this chapter that WSSG based control of the author's ribbed plate is possible if certain conditions are met. The control and disturbance shakers should ideally be placed in the same bin. If this is not possible, then the shakers should be placed in the outer bins so that some degree of control is still attainable. The sensor should ideally be placed in the same bin as the disturbance shaker, but some control is still attainable if it is placed in others. Care should be taken so that the sensor is not placed too close to the ribs due to distortions in the WSSG field near the ribs. Further, the mass of the two shakers should be kept to a minimum to avoid changes to the structural modes.

If these conditions are met then a vibrating simply supported plate with two free ribs can be controlled with WSSG as the minimization quantity.

6 RECOMMENDATIONS AND CONCLUSIONS

The purpose of this section is to sum up the major conclusions presented in this thesis and give recommendations for future work.

6.1 Conclusions

Significant progress has been made on the use of WSSG in active structural acoustic control of simply-supported, clamped, and simply-supported ribbed plates. Attenuation of radiated sound power is achieved by minimizing WSSG at a single point on the plate by optimizing the amplitude and phase of a single control force. This attenuation can be increased by adding a second control force and keeping just one WSSG sensor. The addition of the second control force helps attenuate radiated sound power coming from degenerate or otherwise distorted modes.

A method was derived and analyzed to approximate the four WSSG terms experimentally. This was done using four closely spaced accelerometers whose values were combined to form derivatives using finite difference methods. A method for determining the optimal spacing between the accelerometers was developed and implemented for the authors' specific experimental setup.

It has been shown in many cases that the experimental results closely match computer simulations, but not in all cases. The differences between the experimental results and the

simulations are theorized to have been a result of random noise in the accelerometer signals and distortions in the structural modes which the computer simulations did not account for. These distortions are likely due to structural mode shapes superimposing on top of each other (when their frequencies are close together) and interactions between the plate and the shakers. The computer simulations did not account for these factors and thus predicted much higher attenuation levels than were actually attained.

Despite these differences, significant control was still achieved in many tests. Thus WSSG should be considered as a viable alternative for use as a minimization quantity in active structural acoustic control of a simply supported, clamped and ribbed flat plates. Although it may not be perfect, the ease of implementation and relatively unobtrusive nature of the sensors and actuators makes it more practical to use than most other minimization quantities.

6.2 **Recommendations**

Although significant progress has been made on the experimental use of WSSG in ASAC situations, there are still many areas which could use further investigation. This section contains several observations which the author has made based on his research and recommendations for possible future research work.

6.2.1 The Control Actuators

One of the important pieces of this thesis was the research which went into the development of an appropriate sensor to measure WSSG. In the end it was discovered that the best sensor was an array of closely spaced accelerometers and the use of the finite difference methods to calculate the spatial gradients. However, when this was implemented on the

experimental setups, it was quickly discovered that the measurement of WSSG was highly dependent upon noise in the sensors. This work is shown in Chapter 2.

In order to minimize the noise levels in the experimental set up it was determined that the shakers used as the disturbance and control actuators needed to be able to produce a pure (no noise) forcing signal at low frequencies. Many of the plates used in our setups had resonant frequencies as low as 35 Hz and so it was important to have actuators which could produce a clean forcing signal for frequencies down to 25 Hz. In order to get these clean results it was necessary to use two shakers which had a relatively large mass compared to the mass of the plate (the shakers weighed over 5 kgs); the Labworks ET-126 shaker and the Bruel and Kjaer type 4809 Vibration Exciter. These larger shakers could produce the clean signal that was desired where several smaller shakers were unable to do so.

However these larger shakers had unintended consequences which had not been foreseen; they added mass, stiffness and damping to the plate. This often caused the experimental results to differ from the computer simulations, and to differ between experimental setups as well. The added mass and stiffness of the shakers shifted the natural frequencies of the plate so that they often did not line up with the computer simulations. This was mentioned in Chapter 4 when the frequencies between two different configurations of the clamped plate were compared. Six resonant frequencies were compared and five of them shifted up in frequency when the shakers were placed in configuration two, but one of them inexplicably shifted down. The only difference between the configurations was the positions of the shakers and so moving the shakers around appears to have added mass or stiffness to the plate. Placing the shakers near the center of the plate may possibly cause these effects to be amplified, while placing them near the edges of the plate may minimize these effects.

This effect can also be seen in Chapter 3 when the simply supported plate is studied in configuration two. Figure 3-13 shows the simulated results and Fig. 3-14 shows the experimental results. These results were carefully scrutinized in order to ensure that the same structural modes were being compared across both figures. It is seen that the first two modes (the 1-1 and 1-2 modes) had higher experimental resonant frequencies than the simulation predicted. However, the 2-1, 2-2, 1-4, and 3-2 modes were all shifted down in frequency. These results are not fully understood by the author and further research might be beneficial.

In addition to shifting the natural frequencies of the plate, adding the heavy shakers also caused minor distortions to the structural mode shapes. Mass loading from the shakers was probably not the primary cause of distortion, but the author believes it contributed to the distortion of the structural modes in minor, yet noticeable, ways. This is discussed in Section 4-4, and may have had a more significant effect on the outcome of the control plots than shifting the natural frequencies did.

These effects could be minimized by using different actuators, and future studies in WSSG should investigate the use of other methods of exciting the plate. These could include using smaller shakers, using piezoelectric elements, or other forms of lightweight linear force actuators. Doing this would help WSSG maintain its uniform nature and the author theorizes that this would bring the experimental results better into harmony with the computer simulations. This would be highly desired because the computer simulations showed more attenuation than the experimental results in every test run.

6.2.2 Software Limitations

The control algorithm used in the experimental tests was a modified filtered X-LMS algorithm. This algorithm has been shown to be effective for active noise control situations by a

variety of researchers and was chosen for its highly effective results and ease of adaptation. However, the software used to implement the control algorithm had several limitations based on allocation of DSP memory during usage. One major limitation was the number of taps used for the sys ID measurement. Sys ID was run on broadband noise and the number of taps ranged from 20 to 150. The sample rate of the system ranged from 1000 Hz to 4000 Hz depending on the tests. This means that the bin width for the sys ID ranged anywhere from $\frac{1000Hz}{150Taps} = 6.67$ Hz to $\frac{4000Hz}{20Taps} = 200\ Hz.$ The majority of the tests run for this thesis were done with a 2000 Hz sample frequency and 60 Taps, which gives a bin width of 33 Hz. This worked effectively for most tests, but not all. When particularly bad control results were attained for a single frequency, then the test was re-run with different combinations of sample frequencies and number of taps, in search of a better result. Often better control results were achieved, but at times little improvement was shown. This could be because the Sys ID bins were too large to find the optimal phase for the control shaker.

This could be remedied in one of two ways: increasing the computing memory so that more taps can be used, or change the Sys ID program to run on single frequencies. The second option only works because our tests are run frequency by frequency, and is not an option if broadband noise is to be controlled. Making these changes could improve the control results of the experimental tests performed for this thesis.

6.2.3 Higher Mode Analysis

Research on WSSG has focused, for the most part, on low frequencies. With a few exceptions, the tests have been run only up to a few hundred Hz. This was done because the low frequency range is where ASAC has some of its greatest potential for use in practical situations.

Low frequency acoustic waves are more likely to propagate through walls than high frequency waves and so there is a greater need for active cancelation of low frequency waves than high. WSSG has been shown to work reasonably well at attenuating many of these low frequencies.

However, the transition point between "low" frequency waves (which may need to be attenuated actively) and "high" frequency waves (which may be attenuated passively) is not an exact value and is actual highly dependent upon each individual situation. It would therefore be useful if WSSG were able to attenuate sound power from a radiating plate for frequencies higher than the few hundred Hz which have been studied up to this point.

A few simulations were run on the simply supported plate for higher frequencies and one of these is shown in Fig. 7-1. This simulation has the same plate properties and shaker/sensor configuration as Fig. 3-7. Figure 7-1 shows that WSSG does not do a good job of attenuating these higher resonant frequencies. Research is needed to determine why WSSG does not perform well at the higher modes and if WSSG can be modified in any manner to increase its effectiveness.

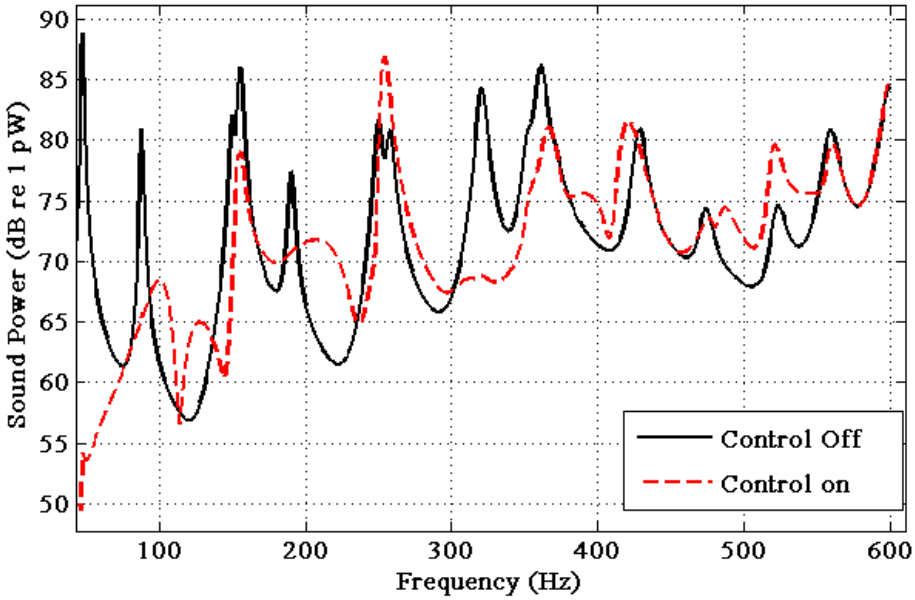

Figure 6-1: Sound Power of a Simply Supported Plate for High Frequencies.

6.2.4 Arbitrary Plate Structures

The analyses presented in this thesis present work done for rectangular and square plates. Computer simulations were run for several different plate sizes, representing many height-to-width ratios. These control plots generally resulted in plots similar to those presented in earlier chapter, and it was shown that WSSG works well on most plate configurations. The experimental tests were limited to plates which were all roughly the same size, due to the nature of the set up. It was shown that WSSG is a viable alternative to other ASAC parameters for these rectangular and square plates. However, research still needs to be done on the use of WSSG on non-rectangular and arbitrary structures.

Limited research was conducted on circular flat plates, but is not presented in this thesis. These tests showed that WSSG was not a good parameter for use as the minimization quantity for circular plates. Many of the structural modes on circular plates were inefficient radiators and volume velocity was shown to be a better indicator of which structural modes contributed to sound radiation.

The use of WSSG on other structures should be investigated. This includes both on other polygons and on arbitrary non-polygonal shapes. These shapes will have vastly different structural modes than the rectangular plates shown in this paper and so the spatial gradients would also be different. Research should be done to see if these spatial gradients continue produce a uniform quantity when summed together. If a uniform quantity is attained then WSSG may perform well on these shapes. If a uniform quantity is not attained then WSSG may not be a good fit as the minimization quantity in ASAC situations.

6.2.5 Room Modes

One additional reason the experimental results may have been different from the computer simulations is acoustic loading of the plate from the room modes of the reverberation chambers. The dimensions of the rooms were given in Chapter 3 and it was noted that several of the room modes fell within the frequency range of the experimental tests. A table showing some of the important axial modes of the large chamber is given in Table 6-1. The small chamber room modes are not shown here but they also contain many frequencies within the range of the experimental tests performed in this thesis.

Table 6-1: Axial Modes of the Small Reverberation Chamber

Length (4.96 m)		Width (5.89 m)		Height (6.98 m)	
Mode	Frequency (Hz)	Mode	Frequency (Hz)	Mode	Frequency (Hz)
1 0 0	34.3	0 1 0	28.9	0 0 1	24.3
2 0 0	68.6	0 2 0	57.8	0 0 2	48.8
3 0 0	102.9	0 3 0	86.7	0 0 3	73.1
4 0 0	137.2	0 4 0	115.6	0 0 4	97.5
5 0 0	171.5	0 5 0	144.4	0 0 5	121.9
6 0 0	205.8	0 6 0	173.3	0 0 6	146.3

It is possible that these room modes may have contributed to some of the distortions seen on the structural modes of the plates. This could be verified/disproved by placing the vibrating plate in an anechoic environment and reproducing some of the results. This would show if the room modes were disrupting the uniformity of the structural modes.

6.2.6 WSSG and Radiation Modes

Fisher *et al.*[8] theorized one possible reason that WSSG is able to attenuate sound power is that the four WSSG terms resemble the most efficient independent acoustic radiation modes of a vibrating simply supported plate at low frequencies. Recent research has begun to question the

relationship between the two quantities. There may still be a connection between them but further research is needed to establish or disprove a relationship. If WSSG is shown to have no connection to independent acoustic radiation modes then attempts should be made to determine if it is better correlated to other quantities such as kinetic and potential energy in the plate.

REFERENCES

1. Snyder, S. D. and Hansen, C. H. "Mechanisms of active control by vibration sources," *J. Sound Vib*., 147, 519–525 (1991).

2. Fahy F. and Gardonio, P, *Sound and Structural Vibration: Radiation, Transmission and Response*, Elsevier, Oxford (2007).

3. Pan, J., Snyder, S. D., and Hansen, C.J. "Active control of far-field sound radiated by a rectangular panel-A general analysis," *J. of the Acoustical Society of America*, 1992: 2056 (1991).

4. Fuller, C.R. "Active control of sound transmission/radiation from elastic plates by vibration inputs: I. Analysis". *J. Sound Vib.,* 1-15 (1990).

5. Fuller, C. R. Hansen, C. H., and Snyder, S. D. "Active control of sound radiation from a vibrating rectangular panel by sound sources and vibration inputs: An experimental comparison". *J. Sound Vib.,* 195-215 (1991).

6. Snyder, S. D. and Tanaka, N. "On feed-forward active control of sound and vibration using vibration error signals," *J. of the Acoustical Society of America*, 94, 2181–2193 (1993).

7. Sors, T. C. and Elliott, S. J. "Volume velocity estimation with accelerometer arrays for active structural acoustic control," *J. Sound Vib*., 258, 867–883 (2002).

8. Johnson, M. E. and Elliott, S. J. "Active control of sound radiation using volume velocity cancellation," *J. of the Acoustical Society of America*, 98, 2174–2186 (1995).

9. Johnson, M. E. and Elliott, S. J. "Volume velocity sensors for active control," *Proc. Inst. Acoust*., 15, 411–420 (1993).

10. Fisher, J. M., "Development of a pseudo-uniform structural velocity metric for use in active structural acoustic control." Master's thesis, Brigham Young University, Provo, Utah (2010).

11. Tanaka, N., Snyder, S. D., Kikushima, Y., and Kuroda, M. "Vortex structural power flow in a thin plate and the influence on the acoustic field". *J. of the Acoustical Society of America,* 2056-2066 (1994).

12. Snyder, S. D., Brugan, N. C., and Tanaka, N. “An acoustic based modal filtering approach to sensing system design for active control of structural acoustic radiation: Theoretical development”. *Mechanical Systems and Signal Processing,* 123-139 (2002).

13. Elliott, S. J. and Johnson, M. E. “Radiation Modes and the Active Control of Sound Power” *J. of the Acoustical Society of America*, 2194 – 2204 (1993).

14. Cunefare, K. A., Currey, M. N. “On the exterior acoustic radiation modes of structures”. *J. of the Acoustical Society of America.* 2320-2312 (1996).

15. Fisher, J.M. Blotter, J. D. Sommerfeldt, S. D. and Gee, K. L. “Development of a pseudo-uniform structural quantity for use in active structural acoustic control of simply supported plates: An analytical comparison”, *J. of the Acoustical Society of America,* 131, 3833 – 3840 (2012).

16. Pavic G. “Measurement of vibrations by strain gauges, Part II: Selection of measurement parameters.” *J. Sound Vib*., 165-188 (1985).

17. Scott, B. L., Sommerfeldt, S. D.. “Estimating acoustic radiation from a Bernoulli-Euler beam using shaped polyvinylidene fluoride film.” *J. of the Acoustical Society of America,* 3475-3485 (1997).

18 Chapra, S. C. and Canale R. P. *Numerical Methods for Engineers - Fifth Edition*. (McGraw-Hill, New York, (2006).

19. Johnson W. R., “Active structural acoustic control of clamped and ribbed plates.” Master’s thesis, Brigham Young University, Provo, Utah (2013).

20. Sung, Chia-Chi and Jan, C. T. “Active Control of Structurally Radiated Sound from Plates” *J. of the Acoustical Society of America,* 370 – 381 (1997).

21. Leissa, A, *Vibration of Plates* (American Institute of Physics) (1993).